Article

Inhibition of A# amyloid growth and toxicity by Silybins: the crucial role of stereochemistry

Michele Francesco Maria Sciacca, Valeria Romanucci, Armando Zarrelli, Irene Monaco, Fabio Lolicato, Natalia Spinella, Clelia Galati, Giuseppe Grasso, Luisa D'Urso, Margherita Romeo, Luisa Diomede, Mario Salmona, Corrado Bongiorno, Giovanni Di Fabio, Carmelo La Rosa, and Danilo Milardi

ACS Chem. Neurosci., **Just Accepted Manuscript** • Publication Date (Web): 31 May 2017

Inhibition of Aβ amyloid growth and toxicity by Silybins: the crucial role of stereochemistry

Michele. F. M. Sciacca[1], Valeria Romanucci[2], Armando Zarrelli[2], Irene Monaco[1], Fabio Lolicato[3,4], Natalia Spinella[5], Clelia Galati[5], Giuseppe Grasso[6], Luisa D'Urso[6], Margherita Romeo[7], Luisa Diomede[7], Mario Salmona[7], Corrado Bongiorno[8], Giovanni Di Fabio[2]*, Carmelo La Rosa[6]* and Danilo Milardi[1]*

[1]Institute of Biostructures and Bioimages—Catania, National Research Council, Via Paolo Gaifami 8, 95126 Catania, Italy.
[2]Department of Chemical Sciences, University of Napoli 'Federico II', Via Cintia 4, I-80126 Napoli, Italy.
[3] Department of Physics, University of Helsinki, P.O. Box 64, FI-00014 Helsinki, Finland.
[4]Department of Physics, Tampere University of Technology, P.O. Box 692, FI-33101 Tampere, Finland.
[5]STMicroelectronics, Stradale Primosole 50, 95121 Catania, Italy.
[6]Dipartimento di Scienze Chimiche, Università degli Studi di Catania, Viale Andrea Doria 6, 95125 Catania, Italy.
[7]IRCCS-Istituto di Ricerche Farmacologiche "Mario Negri", Via Giuseppe La Masa 19, 20156, Milano, Italy.
[8]Institute for Microelectronics and Microsystems- National Research Council, Stradale Primosole 50, 95121 Catania, Italy.

Keywords: chiral drugs, neurodegeneration, natural compounds, neuroprotection, Alzheimer disease

ABSTRACT: The self-assembling of the amyloid β (Aβ) peptide into neurotoxic aggregates is considered a central event in the pathogenesis of Alzheimer's Disease (AD). Based on the "amyloid hypothesis" much efforts have been devoted in designing molecules able to halt disease progression by inhibiting Aβ self-assembly. Here, we combine biophysical (ThT assays, TEM and AFM imaging), biochemical (WB and ESI-MS) and computational (all-atom Molecular Dynamics) techniques to investigate the capacity of four optically pure components of the natural product Silymarin (Silybin A, Silybin B, 2,3-Dehydrosilybin A, 2,3-Dehydrosilybin B), to inhibit Aβ aggregation. Despite TEM analysis demonstrated that all the four investigated flavonoids prevent the formation of mature fibrils, ThT assays, WB and AFM investigations showed that only Silybin B was able to halt the growth of small-sized protofibrils thus promoting the formation of large, amorphous aggregates. Molecular dynamics (MD) simulations indicated that Silybin B interacts mainly with the C-terminal hydrophobic segment ^{35}MVGGVV^{40} of Aβ40. Consequently to Silybin B binding, the peptide conformation remains predominantly unstructured along all the simulations. By contrast Silybin A interacts preferentially with the segments ^{17}LVFF^{20} and ^{27}NKGAII^{32} of Aβ40 which shows a high tendency to form bend, turn and β-sheet conformation in and around these two domains. Both 2,3-Dehydrosilybin enantiomers bind preferentially the segment ^{17}LVFF^{20} but lead to the formation of different small-sized, ThT-positive Aβ aggregates. Finally, *in vivo* studies in a transgenic *C. elegans* strain expressing human Aβ, indicated that

Silybin B is the most effective of the four compounds in counteracting Aβ proteotoxicity. This study underscores the pivotal role of stereochemistry in determining the neuroprotective potential of Silybins and points to Sil B as a promising lead compound for further development in anti AD therapeutics.

Introduction

Alzheimer's disease (AD) is the most widespread form of neurodegenerative disorder affecting elderly people worldwide. Post-mortem analyses of brain tissues from AD patients are characterized by the presence of plaques which contain aggregates of amyloid (Aβ) peptide.[1] In the AD brain, high levels of Aβ40 and Aβ42 peptides result from an abnormal cleavage of the amyloid precursor protein (APP) by the proteases β- and λ-secretase.[2] Although Aβ42 is more prone to form toxic aggregates, Aβ40 is more abundant (it is produced in a 9:1 molar ratio with respect Aβ42).[3] For this reason, and due also to the low solubility of Aβ42 that prevents some biophysical examinations, most cell-free studies have been performed on Aβ40.[4] Although a causal relationship between the morphology of Aβ aggregates and the harshness of the disease still remains to be firmly established, the conversion of Aβ from its soluble, monomeric state into toxic aggregates in the brain[5,6] is commonly believed to be a key event in AD pathogenesis (amyloid hypothesis).[7] Several adverse factors are known to contribute to amyloid aggregation in vitro and in vivo. As an example, abnormal interactions with model membranes have been evidenced to foster Aβ aggregation.[8] Next, mislocated metal ions as Cu(II) or Zn(II), which in physiological conditions contribute to the stability of native proteins,[9,10] may accelerate Reactive Oxygen Species (ROS) production, protein misfolding and aggregation.[11] In particular, accumulating evidence suggests that small-sized, soluble Aβ oligomers occurring during peptide aggregation are cytotoxic whereas mature fibrils are inert.[12] Therefore, a current strategy to treat AD includes the design of new molecules able to inhibit the self-assembly of Aβ.[13,14] To this aim, a number of compounds have been used as inhibitors of Aβ aggregation including peptide beta-sheet breakers,[15–17] antibodies,[18] Congo Red derivatives[19] and osmolytes[20] but always with limited success and often severe side effects. Recent studies have shown that small lipophilic molecules extracted from natural sources, due also to their permeability across the Blood Brain Barrier (BBB) and safe pharmacological profile, are attractive candidates for the treatment of AD.[13,21–24] Several natural molecules as curcumin,[25] scyllo-inostol,[26,27] resveratrol[28] and (−)-epigallocatechin-3-gallate[29] have evidenced antiaggregating and antioxidant effects and are currently under clinical investigation. Among natural molecules Silymarin, a flavonoid complex extracted from milk thistle (*Silibum marianum*), has shown promising neuroprotective effects.[30–33] Silymarin is a combination of some flavonoids found in the fruit, seeds and leaves of milk thistle, and many of these occur as pairs of diastereoisomers (silibinin, isosilybin, silychristin) or enantiomers (2,3-

Dehydrosilybin, DHS), some of which possess very attractive pharmacological properties. Silibinin, the major component of Silymarin, is a diastereoisomeric mixture of two flavonolignans, namely Silybin A (Sil A) and Silybin B (Sil B) in a ratio of approximately 1:1, while the 2,3-Dehydrosilybin is a mixture of enantiomers (DHS A and DHS B).[34] Silibinin prevented oxidative damage and memory impairment in mice treated with Aβ25-35,[35] and may act as an inhibitor of Aβ amyloidogenesis.[36] In many cases the optical purity aspect of silibinin and DHS (Silybins) have been largely neglected, but their stereochemistry could play an extremely important role with interesting pharmacological implications. In this context further studies are needed to single out the molecular basis of the antiaggregating properties of these compounds. Herein we investigate the ability of Sil A, Sil B, DHS A and DHS B, prepared and purified through a convenient approach (Figure 1)[37,38] to bind Aβ and interfere with its aggregation into toxic assemblies. To this aim, we performed tube-tests employing Thioflavin T fluorescence (ThT) assay, SDS-PAGE, TEM-EDX and AFM imaging techniques. An ESI-MS analysis of the small peptides obtained from the proteolytic digestion of Aβ in the presence of Silybins was also performed in order to characterize the effect of each compound in Aβ degradation. The Insulin Degradin Enzyme (IDE) was selected among all the available Aβ degrading enzymes because of its involvement in AD and the in-depth knowledge of IDE degrading activity towards various substrates by our group.[39,40] Molecular Dynamics simulations were also performed to provide detailed energetical and structural information about the interaction of monomeric Aβ40 with the four compounds, indicating that Sil B can effectively bind aromatic/hydrophobic residues of Aβ thus diverting its capability of forming small-sized protofibrillar toxic oligomers. *In vivo* studies were then perfomed to investigate how silybins counteracted the Aβ-induced toxicity. To this end, we used transgenic CL4176 *Caenorhabditis Elegans* strain as a simplified invertebrate prototype of Aβ amyloidogenesis, already employed as a valuable *in vivo* animal model for pharmacological studies.[21,23,41,42] In this strain the expression of human Aβ42 results in the specific accumulation of oligomeric assemblies in the body wall muscle cells which leads to paralysis. Among the four derivatives only Sil B resulted effective in protecting worms against the Aβ toxicity indicating a close relationship between the stereochemistry of the antiaggregating molecules and their mechanisms of action.

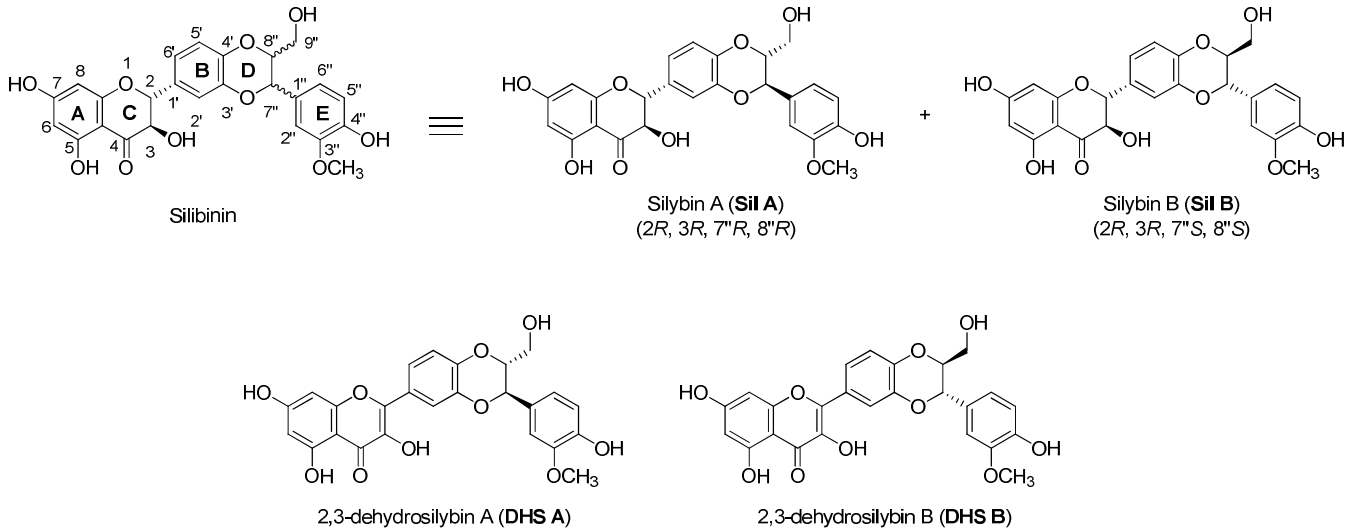

Figure 1. Chemical structures of Silybins (Sil A, Sil B, DHS A and DHS B).

Results and discussion

Sil B abolishes Aβ40 amyloid growth

ThT and WB experiments were first performed to test the antiaggregation properties of the four compounds (Figure 2A-C). Sil B shows a dose-dependent antiaggregation potency (Figure 2C) and at a concentration of 4 μM (peptide/ligand ratio ~ 2.5:1) fully abolishes Aβ40 fiber formation. Sil A also shows a concentration dependent behaviour (Figure 2D). However, although it significantly decreases the total amount of amyloid fibers and slows down the fiber formation process (t_{half} ~ 1050 min) compared with the sample containing only Aβ40 alone (t_{half} ~450 min), it is not able to completely block amyloid growth. Both DHS A and DHS B (Figure 2A) slow down kinetics of amyloid formation (t_{half} ~1300 min and ~1000 min respectively); however it does not reduce significantly the total amount of amyloid formed. These data indicate that all Silybins significantly interfere with the Aβ40 fiber formation process, but only Sil B is able to completely inhibits amyloid fiber formation. ThT assays performed using Aβ42 confirmed the ability of Sil B to interfere with peptide fibrillogenesis (Figure S1 of Supporting Information). The different abilities of the diastereisomers Sil A and Sil B to interfere with the formation of Aβ40 small-sized oligomers were further analyzed by SDS-PAGE/Western blot. In the experimental conditions adopted for ThT assay Aβ40 rapidly form big aggregates that are too large to enter the gel matrix, leading to detect only monomeric, dimeric and trimeric species, as observed elsewhere.[43] Overall, we observe that Sil B is the most active compound in promoting the formation of small oligomers (Figure 2d). This means that Sil B, differently from Sil A, may divert the early stages of the Aβ aggregation process by forming off-pathway intermediates that do not provide ThT fluorescence.

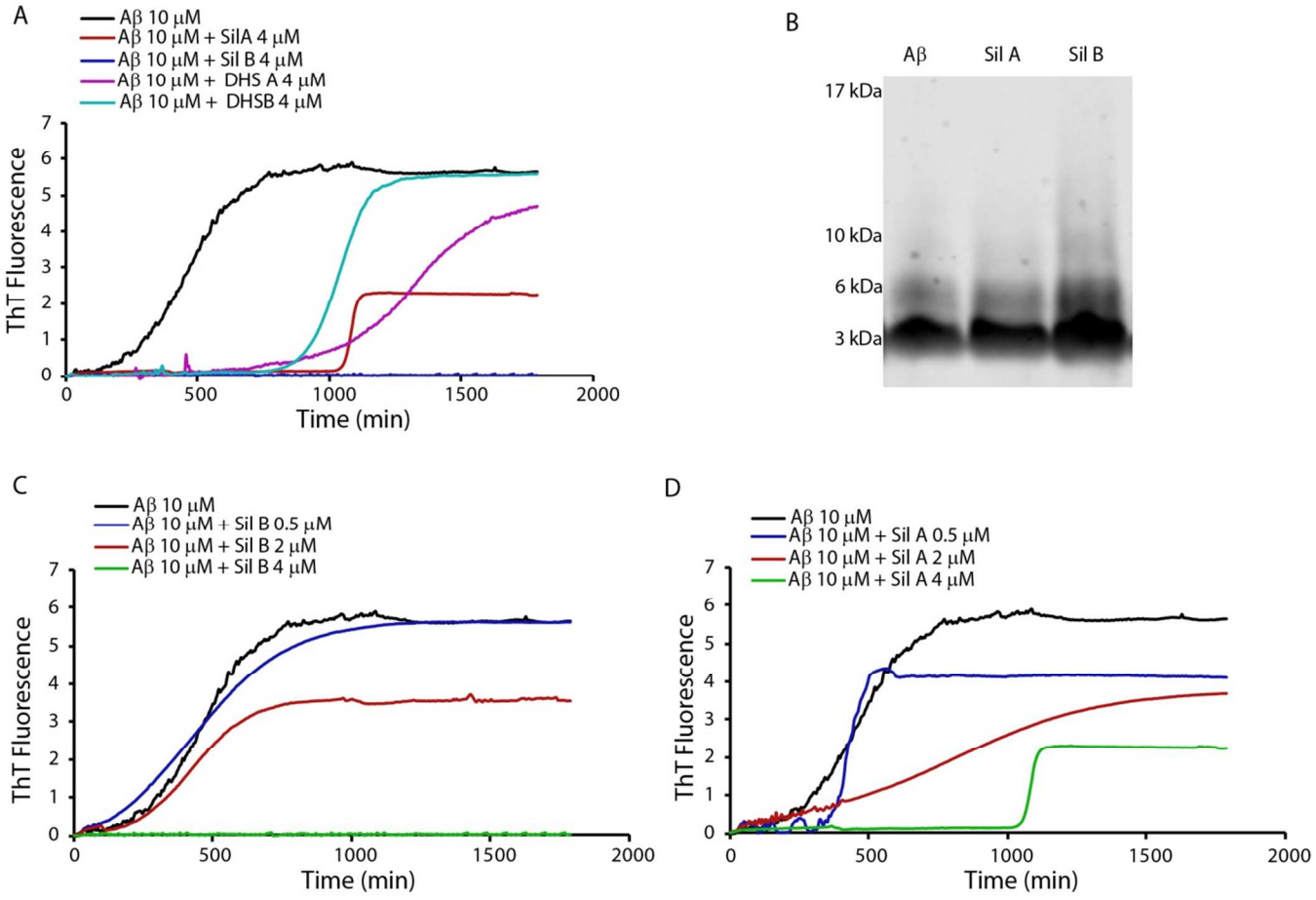

Figure 2. Panel a) ThT traces of samples containing Aβ40 10 μM (black curve) in the presence of 4 μM Sil A, Sil B, DHS A and DHS B; panel b) Representative Western Blot of of small-sized Aβ40. Aβ40 (10 μM) was incubated 1 h of at 37°C alone, with 4 μM Sil A or Sil B. Equal amounts of protein (5 μg) were loaded on each gel lane and immunoblotted with anti-Aβ antibody (6E10). Arrows indicate the Aβ monomers (3 kDa), dimers (~6 kDa) and trimers (10 kDa). ThT traces of samples containing 10 μM Aβ40 (black curve) in the presence of 0.5, 2, and 4 μM Sil B (panel c) and Sil A (panel d). ThT experiments were performed at 37 °C in 10 mM phosphate buffer, 100 mM NaCl, pH 7.4. All results are the average of three experiments.

It has to be reminded that ThT fluorescence may detect only β sheet-rich amyloid protofibrils in solution.[44] Therefore, we used TEM imaging to describe the ability of silybins to interfere with the formation of mature amyloid fibers deposits.[36] Due to the heterogeneous nature of the sample under investigation, a broad-sampling was performed to distinguish amyloid fibrils among the various structures coming from the buffer components (e.g. chlorine and phosphate salts). To this aim, TEM imaging was carried out with a parallel EDX analysis performed on sample areas in which false-fibrillar structures were found. The presence of a nitrogen signal in these spectra was assumed to be indicative of the amyloid nature of the observed fibrils. Figures 3A and 3B show TEM images acquired from a silybin-free sample incubated for 4 days at room temperature. Fibrillar structures have been easily found in different regions of the sample. These fibrils appear like sticks giving a white contrast in the electron

image. They are often observed like bright lines inside a darker area that appear free of other significant features. These bright lines are 5-10 nm large and hundreds of nanometers long. An analogous fibrillar's morphology for Aβ40 was observed elsewhere.[45]

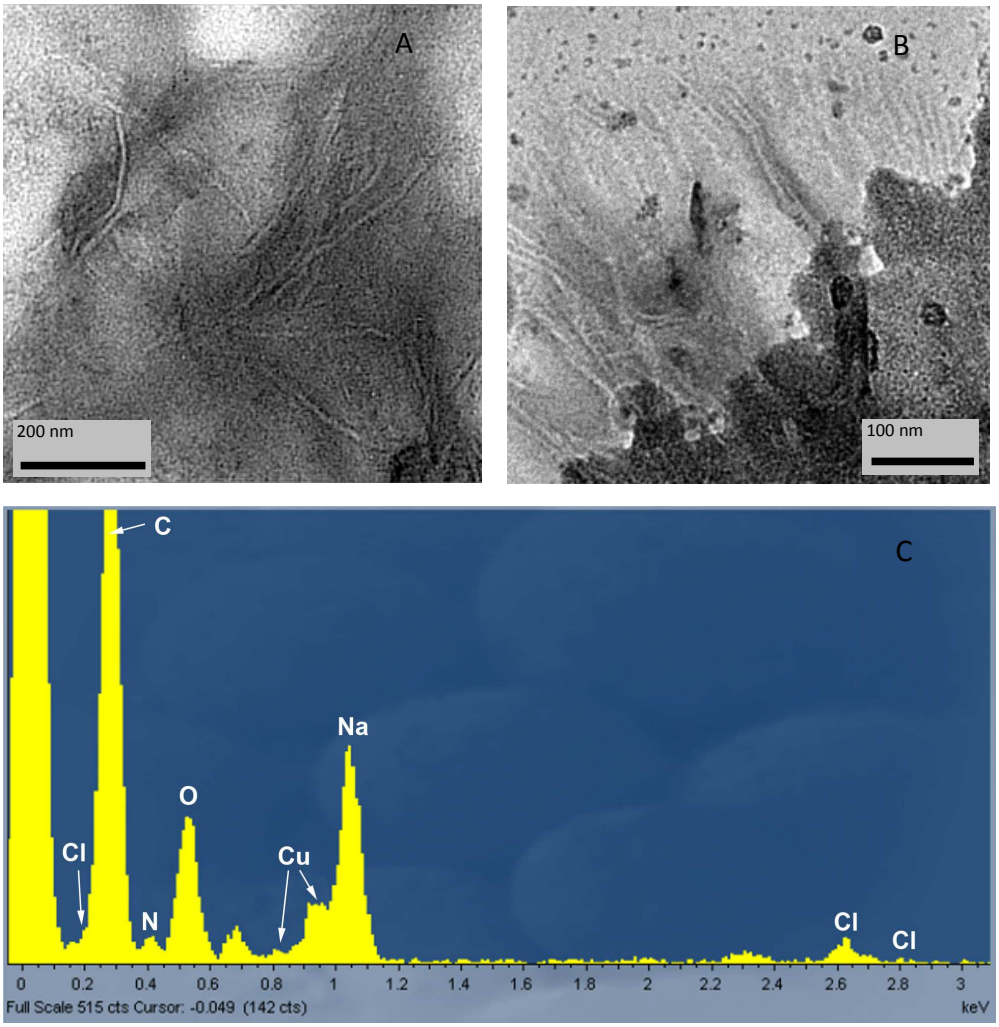

Figure 3. TEM images of fibrils observed in two different areas of a silybin-free sample (panel A and B); the relative EDX spectrum is reported in panel C).

The EDX spectrum captured from this fibril-rich area (Fig. 3c) exhibits a nitrogen signal, as well as the signals derived from the sample holder (e.g. carbon and copper) and from the buffer components (e.g. sodium and chlorine). On the contrary, for samples prepared by incubating the amyloid's solution in the presence of any of the four compounds, no fibrillar structures were observed; in addition, the EDX analysis of the recurrent morphological elements does not give a net evidence of the nitrogen

signal, and only buffer and sample-holder signals were revealed. These data suggest that mature fibrils are not formed in the presence of Silybins and probably they are present on the sample in the prefibrillar amyloid form consisting of a small number of amyloid units with sizes under the resolution limit of the technique or, alternatively, hidden by the structures derived from the other buffer components.

Thus, we used AFM to describe the morphology of Aβ40 aggregates at a higher resolution. Figure 4 shows AFM images and related cross-section for Aβ samples incubated for 24 hours with the four compounds. All systems did not shown any fibril, in accordance to TEM results. Nevertheless, morphologically distinct unstructured aggregates are present in the four samples. In particular, Aβ samples incubated with Sil A self-assemble into small globular aggregates of 1 nm height. By contrast, when incubated with Sil B, Aβ forms larger amorphous aggregates high 10 nm. Peptide samples co-incubated with DHS A exhibits a multi-layer arrangement of dense, irregular globular aggregates with a total height of about 15 nm on average. The morphology of samples incubated with DHS B is similar to the aggregates formed in the presence of Sil A.

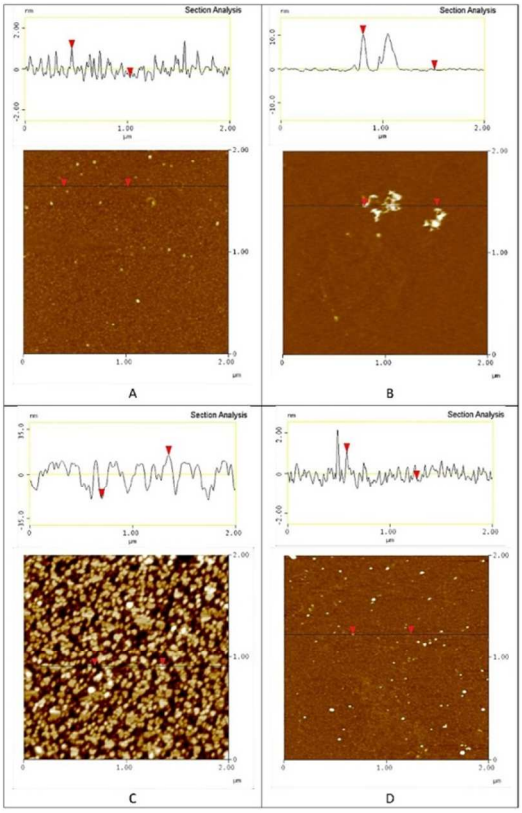

Figure 4. Atomic force microscopy on SiO2 surface image in buffer of 10 μM Aβ40 containing 4 μM Sil A, A); Sil B, B); DHS A, C); DHS B, D). Prior to imaging, the samples were incubated for 24 hours in buffer solution.

Proteolytic activity of IDE versus Aβ40 is altered by Sil A and Sil B.

Next, enzyme degradation assays of Aβ40 by IDE in the presence and in the absence of Sil A, Sil B, DHS A and DHS B have been also carried out by ESI-MS (Figure 5). Aβ is degraded by IDE also in the presence of the compounds, producing the majority of the expected Aβ fragments[46]. However, in the presence of Sil A or Sil B, fragments at m/z 1157.5 and 1325.2, assigned respectively to the QKLVFFAEDVGSNKGAIIGLMVGGVV (doubly charged) and DAEFRHDSGYEVHHQKLVF (doubly charged) segments of Aβ are detected only with very low relative intensities. This result indicates that Aβ degradation by IDE is somehow altered by both compounds in a site specific way (14Q-15K and 18F-19F cleavage sites are the most affected), hinting that Sil A and Sil B may alter the Aβ cryptic fragments produced by the action of this metalloprotease. However, in this experiment we cannot exclude that the compounds may also affect the enzymatic efficacy of IDE by directly binding to the enzyme and in any case we did not observe a detectable difference between Sil A and Sil B modulating activity. For these reasons, further studies on other known IDE substrates might elucidate these points which could be of major interest on their own.

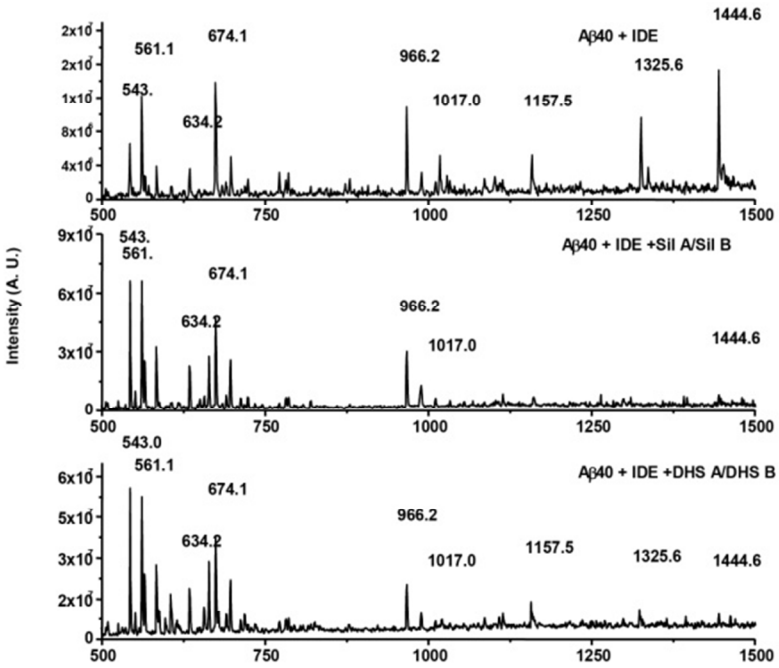

Figure 5. ESI-MS results obtained by enzymatic digestion of Aβ40 by IDE as described in the experimental section. A single degradation time (30 min) is reported and it is possible to note that the Aβ40 molecular peak at m/z 1444.6 has a smaller relative intensity in the presence of both Sil A/ Sil B and DHS A and DHS B, in accordance with a faster Aβ40 degradation by IDE. Moreover, in the case of Sil A/ Sil B, fragments at m/z 1157.5 and 1325.6 are not detected.

Molecular Dynamics of monomeric Aβ40 in the presence of Silybins

ThT assays, TEM, AFM and ESI-MS analysis have evidenced that the four Silybins exhibit different effects on the aggregation propensity of Aβ40. Here, to gain details about the exact mechanisms of inhibition we performed three replicas 1 μs all-atom MD simulations to unveil the interaction modes of Silybins with Aβ40 at a 1:1 molar ratio. First, we investigated the effect of the four compounds on the secondary structure of the peptide. An analysis of the secondary structure profiles (see Figure S2, S3, S4 and S5 in the supporting information) evidences that each of the four compounds has a different effect on Aβ40 conformation. In particular, DHS A has a significant propensity to induce β-sheet conformation in the 15-20 and 30-35 regions of the peptide. By contrast, DHS B induces very stable α-helix conformations in the same regions. In two of the simulated replicas Sil A induces the formation of β-sheets in a region encompassing the N-terminal residues from A2 to F19. Conversely, in the presence of Sil B the peptide adopts a predominantly unstructured conformation in all the three replicas simulated. This singular effect of Sil B is consistent with the average radius of gyration (Rg) calculated for Aβ40 in presence of four molecules (figure S6 in the supporting information) and with circular dichroism (CD) experiments (figure S7 in the supporting information). In fact, the average Rg of the peptide/Sil B system was approximately 1.28 nm whereas, in all the other three systems, (e.g. Sil A, DHS A and DHS B) Rg was about 1.2 nm. To further identify which of the possible binding sites on the Aβ40 monomer may play a major role in driving these conformational changes, we calculated the total interaction energy profile along the peptide sequence for the four systems investigated (Figure 6). Specifically, aromatic residues F19 and F20 provide very favorable binding sites either for both DHS A and DHS B.

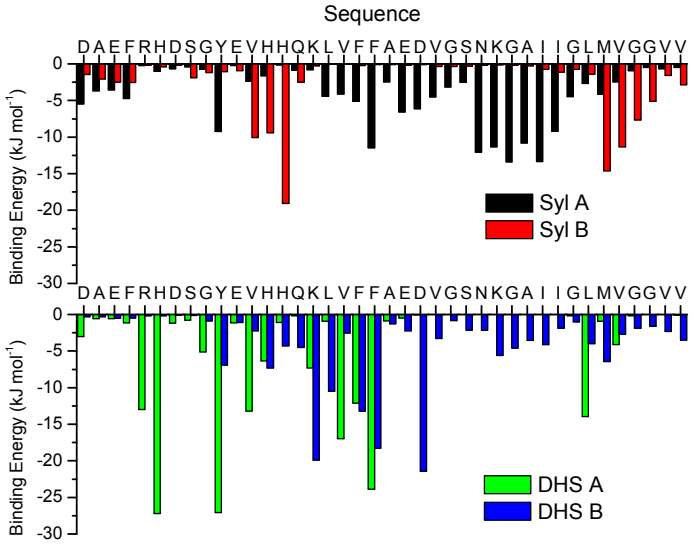

Figure 6. Total binding energy of Sil A, Sil B (upper panel), DHS A and DHS B (lower panel) *vs.* amino acid sequence of Aβ40. Binding energy profiles were calculated by averaging three independent simulations at 37°C and 0.1 M of NaCl.

However, one of the two enantiomers (DHS A) strongly interacts also with E3, H6 and Y10. Other hydrophobic contacts are also observed (L33). There is also a strong electrostatic interaction involving DHS B and D23. Sil A shows a significant binding energy with the hydrophobic residues F20 and N27-I31. By contrast, Sil B shows a high interaction energy with the V12 – H14 and M34 – V39 segments. In particular, this amino acid sequence lies in a region with a high amyloidogenic propensity (see Figure S8 of Supporting Information).[47] A number of reports have demonstrated that any disturbance in intramolecular aromatic (π-π stacking) and hydrophobic interactions may significantly impact amyloid aggregation.[48–50] Moreover, significant antiamyloidogenic properties have been reported for those molecules that bind the U-bend forming the D23-K28 salt bridge which is important in the stabilization of intermolecular β-sheets.[24,51] The whole of the results from molecular dynamics simulations suggest that the large number of binding sites explored by the four Silybins may lead to a large number of different routes along the amyloid formation pathway. However, based on the antiamyloidogenic potential of Sil A and, more significantly, of Sil B evidenced by ThT assays (see Figure 2) we will mainly focus on these two diastereoisomers. Figure 7 reports two representatives snapshots of the binding modes of Sil A and Sil B with Aβ40. In particular, Figure 7 A shows the interaction of the residue Y10 with Sil A. The β-sheet rich N-terminal segment of the peptide is represented as a yellow strand. Figure 7 B shows the preferential binding of Sil B with the C-terminal part of the peptide which remains predominantly unstructured.

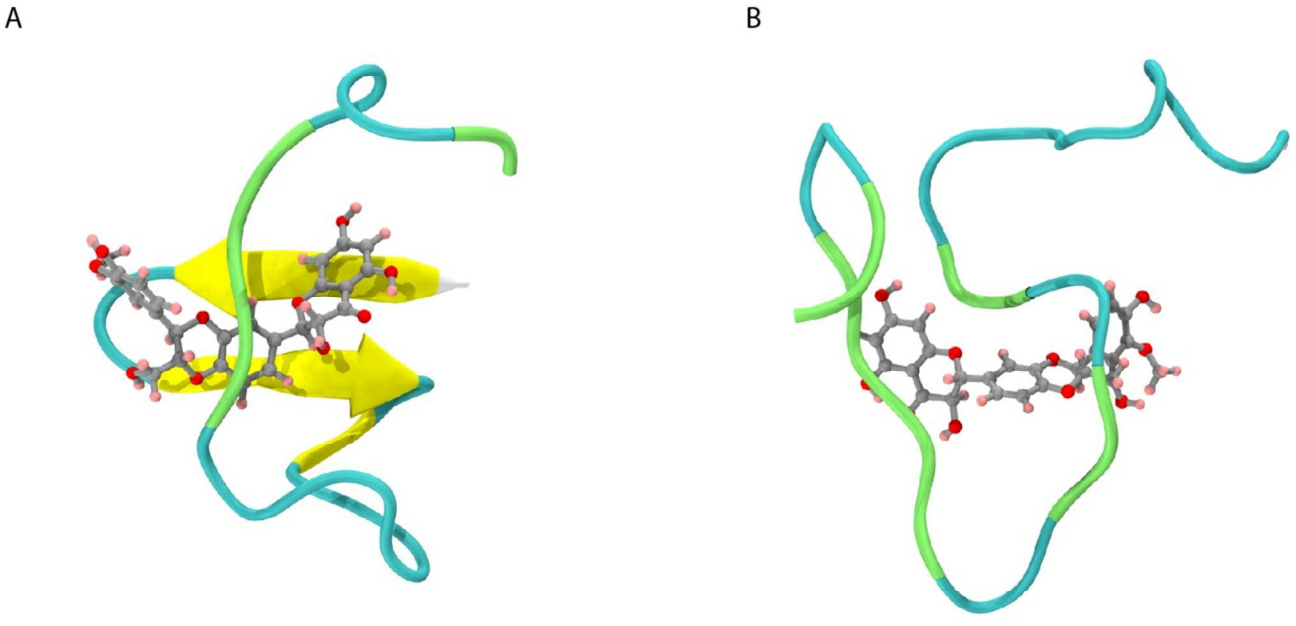

Figure 7. Representative snapshots of some binding modes of Aβ40 with Sil A (A) and Sil B (B). Sil A and B are represented as sticks (color code: light grey, Carbon; red, Oxygen; light red Hydrogen). β-sheets are represented in yellow.

Differently from the two enantiomers DHS A and DHS B which are both characterized by a mostly planar structure, Sil A and Sil B have a flexible, "saddle-like" structure. Moreover, in Sil B, the steric hindrance due to the presence of the OH moiety linked to the D group is expected to prevent the free rotation of the aromatic ring (E group). This hypothesis is confirmed by calculating distance between the 9"-OH and 3"-OCH_3 groups along the whole simulations (Figure 8). Differently from Sil A, for which this distance fluctuates within the range 4- 8 Å (upper panel) in Sil B this distance it has a constant value of 6.3 Å. Thus, the aromatic group of Sil A is flexible and this makes the molecule more available to interact with aromatic groups as F19 and F20 and with the other hydrophobic residues. By contrast, in Sil B this interaction is not possible and interactions with the hydrophobic C-terminus prevail.

As evidenced by TEM analysis, the interactions of each of the four molecules with the peptide are able to prevent amyloid growth into fully mature fibers. However, ThT analysis reveals that DHS A, DHS B and Sil A slow down the aggregation process but do not prevent the formation of amyloid-like protofibrils. This evidence is consistent with the hypothesis that all the investigated compounds, although with different mechanisms, are able to interfere with the Aβ40 aggregation pathway. AFM images confirm this hypothesis and evidence how different morphology of aggregates may be observed for peptide samples incubated with DHS A, DHS B Sil A. On the other side, 4 μM Sil B completely abolishes the growth of ThT positive aggregates in tube tests and lead to the formation of large, amorphous aggregates. To ascertain whether these aggregates are inert we conducted specific toxicity assays *in vivo*.

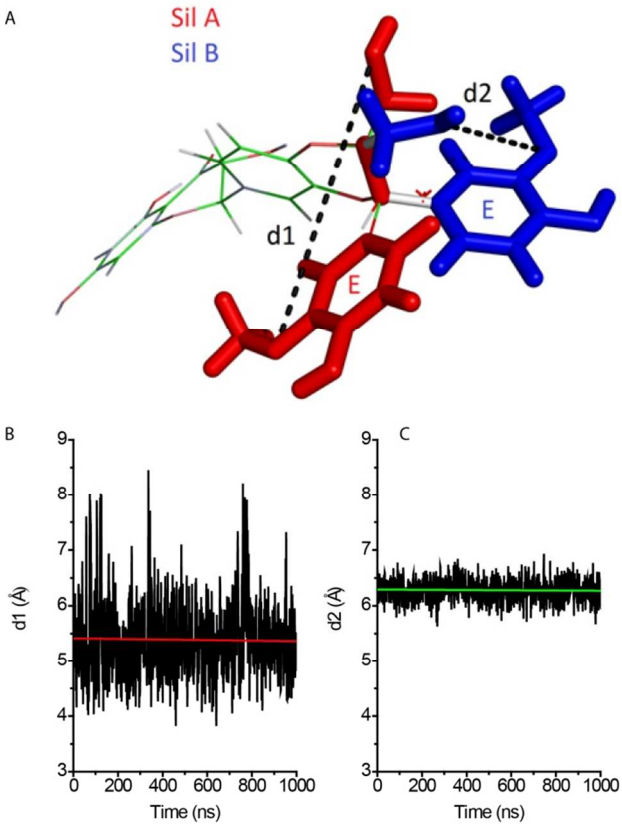

Figure 8. a) 3D representation of an overlay of Sil A (red) and Sil B (blue) structures. The OH groups linked to 9"C atom and the entire E aromatic rings are represented as sticks. The remaining parts of the two molecules are represented as superimposed wires. The distances between the two oxygen atoms of the 9"-OH and 3"- OCH_3 groups are indicated as d1 (for Sil A) and d2 (for Sil B). The variations of d1 and d2 over the simulation time are reported in panel b and c, respectively.

Protective activity of DHS A, DHS B, Sil A and Sil B on Aβ-induced toxicity.

The ability of Silybins to increase the lifespan of *C. elegans* has been investigated elsewhere.[52] Here we employed the transgenic CL4176 strain, in which the paralysis phenotype is specifically caused by the deposition of oligomeric Aβ42 in the body muscle cells and no fibrillar amyloid aggregates are formed. The worms were treated with 50 µM of each compound 12 h after the Aβ transgene induction and their paralysis was scored 24 h later. As shown in Figure 9, among the four derivatives only Sil B completely abolished the CL4176 worms' paralysis (43.1±0.07% of paralyzed worms for vehicle-fed CL4176 and 3.7±0.01% for Syl B-fed worms, $p<0.0001$, one-way Anova). It restored the percentage of CL4176 paralyzed worms at a level comparable to that scored for CL802 worms which did not express Aβ42 (3.7 ±0.44 % of paralyzed worms for vehicle-fed CL802). In the same experimental conditions, DHS A reduced the paralysis by 60% (17.2±0.1%, $p<0.0001$ *vs*. vehicle-fed CL4176, one-way Anova) and DHS B by 20% (34.7±0.2, $p<0.001$ *vs*. vehicle-fed CL4176, one-way Anova), whereas Sil A was ineffective (Figure 9). The four derivatives at the same concentration had no effects in transgenic CL802 control worms (data not shown).

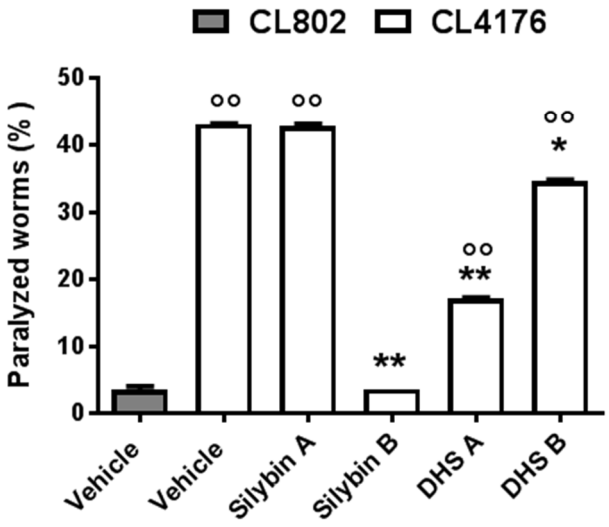

Figure 9 Effect of the four derivatives on the paralysis caused by Aβ42 expression in CL4176 transgenic *C. elegans* strain. CL802 nematodes, which did not express Aβ42, were used as control. Egg-synchronized worms were placed at 16°C on fresh NGM plates seeded with OP50 *E. coli* and the temperature was raised 60 h after plating. Twelve h later, worms were fed 50 μM of Sil A, Sil B, DHS A or DHS B and the number of paralyzed worms was scored after 24 h. Data are percentages ± SE of paralyzed worms compared to vehicle-treated ones (100 worms/group, three independent assays).* $p<0.001$ and **$p<0.0001$ *vs.* CL4176 vehicle fed worms; °°$p<0.0001$ *vs.* CL802 vehicle fed worms, according to one-way Anova and Bonferroni *post hoc* test.

The ability of silymarin to act as potential hormetin preventing age-related adverse effects and protecting C. elegans against the Aβ-induced toxicity have been already reported.[53] Different mechanisms of action has been proposed to be involved in the action of this compound, including the promotion of antioxidant responses, the activation of kinases involved in cell signaling pathways as well as an anti-inflammatory response. [54] To gain insigth into the mechanisms underlying the protective action exerted by Sil B, DHS A and DHS B their effects of on Aβ expression/degradation and oligomerization were evaluated by carrying out dot blotting experiments on lysates of worms treated with 50 μM of each compound for 24 h. To this end, anti-total Aβ antibody WO2, and A11 and OC conformation-selective antibodies, recognizing different classes of quaternary structures[55], were employed. A significant 35% reduction of the total Aβ level was observed in worms treated with Sil B, DHS A and DHS B, but not Sil A (Figure 10 A-B), indicating a relationship between the ability of these compounds to affect the Aβ synthesis/degradation and protect against the Aβ-induced toxicity. The reduction of total Aβ level was accompanied by a significant 50% reduction of A11-reactive oligomers in CL4176 worms treated with Sil B and DHS B (Figure 10 E-F) whereas no effect was observed in the OC-immunoreactive signal (Figure 10 C-D). These results indicate that, whereas the protective effect of DHS A can be ascribed to its ability in reducing total Aβ levels, for Sil B and DHS B an additional

effect on the soluble pre-fibrillar oligomers may be involved indicating a possible relationship between the chemical structure of sylibin derivates and their mechanisms of action in vivo.

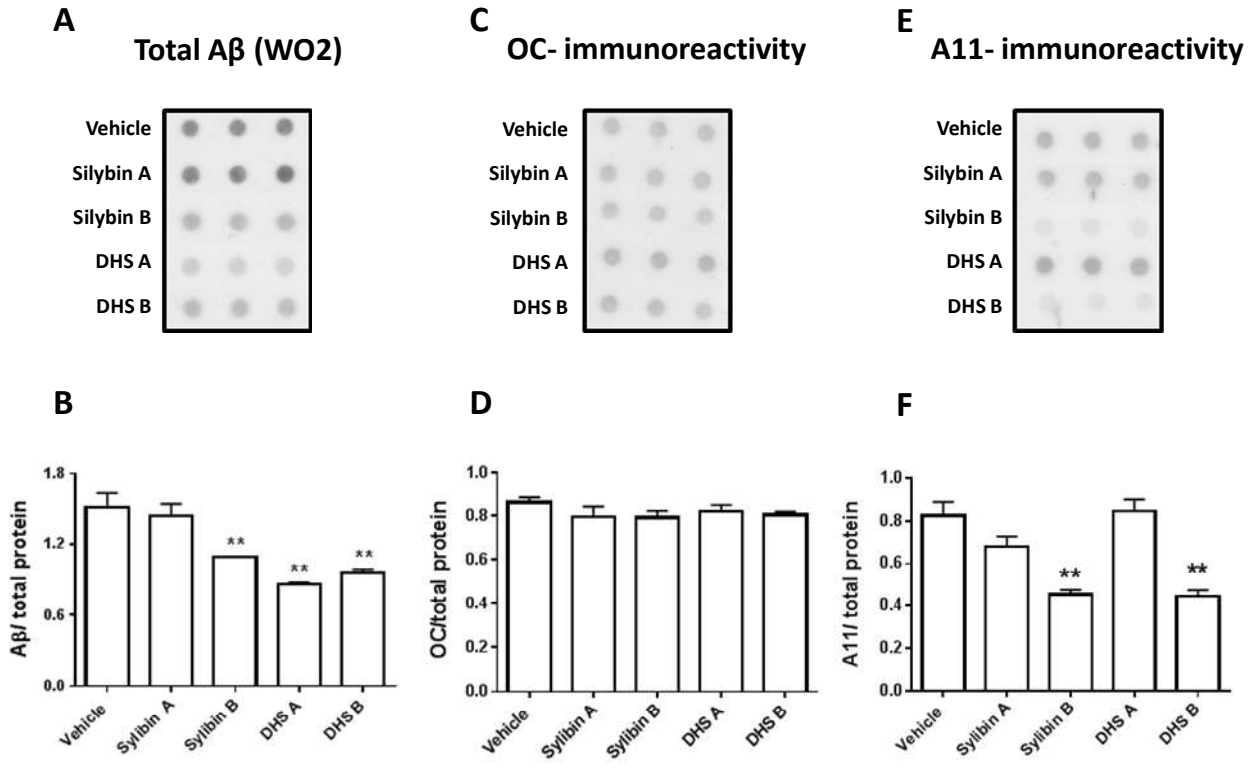

Figure 10. Effects of Sylibin A, Sylibin B, DHS A and DHS B on total and oligomeric Aβ. Representative dot blot of (A) total Aβ (WO2), (C) OC-immunoreactive assemblies and (E) A11-immunoreactive oligomers in CL4176 transgenic worms treated with vehicle or 50 μM Silybins for 24 h. Equal amounts of protein from worm lysates (5 μg) were spotted in triplicate. Total proteins on the blotted membranes were stained using 0.1% Ponceau Red solution and were used to normalized the immuno-specific signal for protein loading. Immunoreactive signal for (B) WO2 total Aβ, (D) OC-recognized assemblies and (F) A11-positive oligomers. Data are the mean volume of the immunoreactive band/total protein ± SE from two independent experiments. **$p < 0.01$ CL4176 worms fed vehicle (one-way Anova and Bonferroni post hoc test).

Conclusions

Conclusively, a battery of biophysical methods coupled with all-atom molecular dynamics simulations has allowed to characterize the interactions of Sil A, Sil B DHS A and DHS B with Aβ40. TEM imaging evidenced that all the four compounds may significantly alter the aggregation pathway of the peptide preventing its ability to form fully mature fibers. However, an analysis of the ThT aggregation traces evidenced that low amounts (4 μM) of DHS A, DHS B and Sil A slow down the aggregation process of

Aβ40, whereas Sil B fully abolished amyloid aggregation. However, since ThT assays are sensitive to β-sheet rich, amyloid-like prefibrillar aggregates, they are less informative about the presence of amorphous aggregates. To address this issue we conducted AFM analysis on peptide samples incubated with the four compounds. The microscopic analysis evidenced that, in the presence of Sil B, Aβ40 produces large, amorphous aggregates, whereas Sil A and DHS B divert the aggregation pathway to smaller aggregates and DHS A to multilayer arrays. Further toxicity assays revealed that Sil B significantly protects transgenic *C. elegans* from the toxicity induced by Aβ suggesting that it is able to interact with toxic oligomers *in vivo*. The large amorphous aggregates formed in vitro and detected by AFM are largely innocuous. Conversely, Sil A is completely ineffective. An inspection of all-atom molecular simulations conducted on Aβ40/Sil A and Aβ40/Sil B systems revealed that Sil B has a specific affinity to the C-terminal domain of the peptide which, in the presence of the compound, remains unstructured along the entire simulation. By contrast, Sil A, binds preferentially the aromatic residues F19 and F20 and has a lower affinity with the C-terminal residues of the peptide. This different behaviour has to be mainly ascribed to the methoxyphenol group which, in Sil A is free to rotate around the C-C bond linking it with the dioxane moiety, whereas in Sil B is blocked because of steric hindrance. Although further *in vivo* studies are necessary to fully validate its therapeutic potential our work identify Sil B as the most potent antifibrillogenic and anti-oligomeric component of silymarin and proposes it as a promising anti AD drug candidate and indicate that a deep knowledge of the stereochemistry of optically active compounds is a not negligible pre-requisite in designing effective antiaggregating compounds.

Materials and Methods

Chemicals. Silibinin was purchased from Sigma-Aldrich. HPLC grade MeCN, MeOH were purchased from Carlo Erba Reagents. Unless otherwise indicated, all chemicals were obtained from Sigma – Aldrich. Sil A and Sil B were separated from commercial Silibinin using the preparative HPLC method. The starting Silibinin solution was prepared by dissolving and sonicating the accurately weighed compound in THF. The obtained solution (ca 140 mg/mL) was then applied to Nylon filters (pore size = 0.45 μm). A 500 μL volume of the Silibinin solution was mixed with 500 μL of the mobile phase and then applied to the chromatographic system. Sil A and Sil B peaks were collected manually. The preparative HPLC purification was performed with a Shimadzu LC-8A PLC system equipped with a Shimadzu SCL-10A VP System control and Shimadzu SPD-10A VP UV-VIS Detector. A Phenomenex Gemini C18-110A preparative column (10-μm particle size, 250 mm × 21.2 mm i.d.) was used, and the mobile phase of H_2O/MeOH/MeCN (60:35:5, v/v/v), containing 0.1% of TFA, was delivered

isocratically at 12 mL/min. The chromatograms were monitored at 288 nm. The HPLC system was controlled by LC Real Time Analysis software (Shimadzu Corporation). Starting from purified diastereoisomers (Sil A and Sil B), it was possible to obtain the two enantiomers of 2,3-Dehydrosilybin in good yields and that were optically pure using an efficient MW oxidation procedure. A solution of Sil A or Sil B (1 g, 2.1 mmol) in 6 mL of DMF and KOAc (610 mg, 6.22 mmol) was placed in a 10 mL glass tube. The tube was sealed with a Teflon septum, placed in the microwave cavity and irradiated. The reaction mixture was held at this temperature for the required time. After the irradiation period, the reaction vessel was cooled rapidly to ambient temperature by gas jet cooling. The solvent was removed under vacuum and the crude material was purified by chromatography over a pre-packed column RP-18 (Biotage® Snap cartridge KP-C-18-HS 25 g) on a Biotage® Isolera Spektra one eluting with a ternary mixture of $CH_3OH/CH_3CN/H_2O$ containing increasing proportions of CH_3CN (from 4:1:5 to 4:3:3, v/v/v).

ThT Measurements. Aβ40 fiber formation kinetics was measured by using Thioflavin T (ThT) assays. Samples were prepared by adding 1 μL of peptide stock solution (250 μM in NaOH 1 mM) to 100 μL of 10 mM phosphate buffer solution (pH 7.4, 100 mM NaCl, containing 20 μM ThT) to obtain a final concentration of 10 μM Aβ40. An opportune amount of Silybins, from stock solutions, were added to the samples to obtain a final concentration in the range of 0.5 – 4 μM. Experiments were carried out in Corning 96 well non-binding surface plates. Time traces were recorded using a Varioskan (ThermoFisher, Walham, MA) plate reader using a λ_{ecc} of 440 nm and a $\lambda_{em}$of 485 nm at 37 ^{o}C, shaking the samples for 10 seconds before each read.

Western Blot Analysis. Gel electrophoresis followed by western blotting experiments were performed on Aβ40 samples incubated (T=37 °C) at different times with the four derivatives at a 1:5 peptide/ligand ratio. Peptide samples (10 μl) were separated onto a 4-12% Bis-Tris gel, (Invitrogen). After separation (160 V), proteins were transferred onto a nitrocellulose membrane and blocked with 3% w/v bovine serum albumin (BSA) for at least 2 hours at room temperature. Membranes were blotted at 4 °C overnight with a primary mouse monoclonal antibody (6E10, 1: 1000, Covance, Princeton NJ, USA) in a solution of 2% BSA (w/v in TBS-T). Next, secondary goat anti-mouse antibody labeled with IRDye 800 (1:25.000 Li-COR Biosciences) were added at room temperature for 45 min. Hybridization signals were detected with the Odyssey Infrared Imaging System (LI-COR Biosciences).

Trasmission Electron Microscopy (TEM). Electron Microscopy analysis was performed on samples prepared by adding an appropriate aliquot of each Silybin solutions to a 10 μM Aβ40, containing Thioflavin-T at a concentration of 20 μM. The Silybin concentration was 50 μM for all samples. The resulting solutions were then incubated for 4 days at 25 ºC. For comparison, a Silybin-free sample was

analyzed. After incubation, all samples were stored at -20 ºC until use. For the electron microscopy analysis, 3 μL of the freshly thawed samples were dispensed on carbon-coated EM copper grids. After dispensing, grids were stored in air (class 1000 clean room) for 24 hours to assure a complete evaporation of the volatile components. EM analysis was performed on the dried grid immediately after preparation. TEM analysis was performed with a Jeol JEM 2010 electron microscope operating at 200KV accelerating voltage and equipped with an Oxford Energy Dispersive X-ray spectrometer (EDXS).

Atomic Force Microscopy (AFM). AFM images of all samples were obtained in contact mode on a NanoScope III (Veeco/Digital Instruments (DI), Santa Barbara, CA) atomic force microscope. Measurements were recorded at room temperature on a monocristalline silicon substrate in Milli-Q water using a liquid cell (DI). A spring constant of about 0.06 N/m of a non conductive silicon nitride tip, was employed for measurements with a scan rate of 0.7-1 Hz and a load force < 100 pN. All images shown are flattened raw data. Cross-sections were used to analyse the height of the observed aggregates.

ESI-MS. ESI-MS experiments were performed by using a Finnigan LCQ DECA XP PLUS ion trap spectrometer operating in the positive ion mode and equipped with an orthogonal ESI source (Thermo Electron Corporation, USA). The mass spectrometer operated with a capillary voltage of 46 V and capillary temperature of 250 ^{o}C, while the spray voltage was 4.3 kV. Aβ40 peptide (10 μM) and Silyibins (4 μM) were incubated for 1 hour at pH 7 in pure water at room temperature.

C. Elegans Studies. The transgenic CL4176 strain (smg-1(cc546ts)I; dvIs27[pAF29 (myo-3/Aβ1–42/let UTR)+pRF4 (rol-6(su1006)]) expressing human Aβ42 in the body-wall muscle and the control CL802 strain (smg-1(cc546) I; rol-6(su1006) II) were obtained from the Caenorhabditis Genetic Center (CGC, USA) and propagated on solid Nematode Growth Medium (NGM) seeded with OP50 E. coli (CGC, USA) for food.[21] Age-synchronized worms were obtained by transferring nematodes to fresh NGM plates to reach maturity at three days of age and lay eggs overnight. Isolated hatchlings from the synchronized eggs were placed at 16°C on fresh NGM plates (35 x10 mm culture plates, 100 worms/plate) seeded with OP50 E. coli. Aβ42 expression was induced by putting worms at 24°C, 54 h after plating. Worms were treated 18 h after the temperature rise (at L3 larval stage) with 50 μM of each compound (100 μL/plate), or 50 μM tetracycline hydrochloride (Fluka, Switzerland) as positive control.[23] All compounds were freshly dissolved at 25 mM in dimethylsulfoxide (DMSO) and then diluted in water before use. DMSO concentration did not exceed 1% (vol/vol) in final solution. Control worms received a 1% DMSO diluted in water (Vehicle). Paralysis of the nematodes was evaluated after 24 h, at the L4 larval stage, by scoring worms that did not move or only moved their head when gently touched with a platinum loop.

Aβ expression. Synchronized CL4176 worms were fed with vehicle or 50 μM Sylibin derivatives as previously described. Twenty-four 24h later nematodes were collected and washed twice with M9 buffer (1100 x g for 3 min) to eliminate bacteria. Worms were re-suspended in lysis buffer (5.0 mM NaCl, 5.0 mM EDTA, 1.0 mM dithiothreitol and protease inhibitor mixture in 25 mM Tris/HCl buffer, pH7.5) and homogenized using a TeSeE homogenizer (Bio-Rad) with acid-washed glass beads (Sigma)20. Equal amount of proteins (5μg) were spotted on nitrocellulose membranes and then incubated with an anti-Aβ mouse monoclonal antibody, clone WO2 (1:1000, Millipore), recognizing amino acid residues 4–10 of Aβ (1:1000, Millipore). The membranes were incubated with two different anti-conformational antibodies: the rabbit polyclonal A11 antibody recognizing prefibrillar oligomers (1:1000 dilution, Biosource, USA)[56] and the rabbit polyclonal OC antibody recognizinganti-amyloid fibrils as well as Aβ fibrillar oligomers (1:1000 dilution, Chemicon).[35] To minimize background staining due to non-specific membrane-binding of the antibody, the membranes were saturated for 1 h at room temperature by incubation with 10 mM PBS, pH 7.4 containing 0.1% (v/v) Tween 20, 5% (w/v) low-fat dry milk powder and 2% (w/v) bovine serum albumin. Peroxidase-conjugated anti-mouse IgG (1:20.000, Sigma) and peroxidase conjugated anti-rabbit IgG (1:20.000, Sigma) were used as secondary antibodies. A 0.1% Ponceau Red solution (Sigma Aldrich) was used to stain the blotted membranes for total protein visualization. The mean volumes of dot-blot immunoreactive spots and of Ponceau-dyed spots were analyzed using Quantity One 1-D Analysis Software (Bio-Rad). The data were expressed as the mean volume of the immunoreactive spot/volume of total Ponceau-dyed proteins in the spot±SE.

Molecular Dynamics. Molecular dynamics simulations were performed by using force field CHARMM36.[57] The initial protein structure used was the NMR structure of Aβ40 in an aqueous environment (pdb ID: 2LFM).[58] It was first energy-minimized using the method of steepest descents. Pre-equilibration was performed in the NPT ensemble for 100 ns to stabilize the structure in solution. The monomeric structure thus obtained was used as the starting configuration of all other systems. The parameters for the Sil A, Sil B, DHS A and DHS B were obtained by using the SwissParam web-server.[59] The partial charges were refined through the employ of PyRED web-server and g09.RevE.01 (Gaussian) software by using MP2/6-31G(d) level of theory.[60,61] Water molecules were described using the TIP3P model.[62] The temperature was kept constant at 310.15 K for all simulations to mimic the experimental setup by using a Nose´-Hoover thermostat[63,64] with a coupling constant of 1 ps. The temperatures of the solute and solvent were controlled independently. Whereas the pressure was maintained constant in all three dimensions at 1 atm by employing the Parrinello-Rahman barostat[65,66] with a pressure coupling constant of 5 ps and a compressibility of $4.5 \times 10^{-5} bar^{-1}$. Long-range electrostatic interactions beyond the nonbonded interaction cutoff of 1.2 nm were treated by using the particle mesh

Ewald scheme.[67] The LINCS algorithm[68] was used to constrain hydrogen bonds, allowing a time step of 2 fs. Periodic boundary conditions were used in all three directions. Three different atomistic simulations were carried out for each system by using GROMACS 5.1.2[69] and were analyzed together with VMD software[70] The binding energies were calculated with the gmx energy GROMACS tool by summing up the coulomb and Leonard Jones interactions.

Supporting Information.

Secondary structure evolution of three independent replicas of Aβ40 with Sil A, Sil B, DHS A and DHS B; Gyration radius of Aβ40 in the presence of Sil A, Sil B, DHS A and DHS; amyloidogenic propensity of Aβ40.

Author information

Corresponding Authors

* clarosa@unict.it; * difabio@unina.it; *danilo.milardi@cnr.it

Acknowledgment

This work was financially supported by MIUR PRIN grant n. 20157WZM8A, Banca IntesaSanpaolo and Fondazione Sacchetti.

Author Contributions:

MFMS performed ThT assays; VR purified Sylibinin; AZ purified DHS A and DHS B; IM performed Western Blot experiments; FL performed molecular dynamics simulations; NS prepared samples for TEM imaging; CG analyzed TEM images; GG performed mass spectrometry experiments; LDU performed and analyzed AFM experiments; MR performed dot blot assays; LD performed and analysed in vivo experiments; MS designed and analysed in vivo experiments; CB performed TEM analysis; GDF designed the research, CLR analysed molecular simulations and designed the research, DM designed the research and wrote the paper.

References

(1) Blennow, K., de Leon, M. J., and Zetterberg, H. (2006) Alzheimer's disease. *Lancet Lond. Engl. 368*, 387–403.
(2) Hamley, I. W. (2012) The Amyloid Beta Peptide: A Chemist's Perspective. Role in Alzheimer's and Fibrillization. *Chem. Rev. 112*, 5147–5192.
(3) Qiu, T., Liu, Q., Chen, Y.-X., Zhao, Y.-F., and Li, Y.-M. (2015) Aβ42 and Aβ40: similarities and differences. *J. Pept. Sci. Off. Publ. Eur. Pept. Soc. 21*, 522–529.

(4) Attanasio, F., De Bona, P., Cataldo, S., Sciacca, M. F. M., Milardi, D., Pignataro, B., and Pappalardo, G. (2013) Copper(II) and zinc(II) dependent effects on Aβ42 aggregation: a CD, Th-T and SFM study. *New J. Chem. 37*, 1206–1215.
(5) Yankner, B. A., Duffy, L. K., and Kirschner, D. A. (1990) Neurotrophic and neurotoxic effects of amyloid beta protein: reversal by tachykinin neuropeptides. *Science 250*, 279–282.
(6) Terzi, E., Hölzemann, G., and Seelig, J. (1997) Interaction of Alzheimer beta-amyloid peptide(1-40) with lipid membranes. *Biochemistry (Mosc.) 36*, 14845–14852.
(7) Hardy, J. A., and Higgins, G. A. (1992) Alzheimer's disease: the amyloid cascade hypothesis. *Science 256*, 184–185.
(8) Pannuzzo, M., Milardi, D., Raudino, A., Karttunen, M., and Rosa, C. L. (2013) Analytical model and multiscale simulations of Aβ peptide aggregation in lipid membranes: towards a unifying description of conformational transitions, oligomerization and membrane damage. *Phys. Chem. Chem. Phys. 15*, 8940–8951.
(9) Manetto, G. D., Rosa, C. L., Grasso, D. M., and Milardi, D. (2005) Evaluation of thermodynamic properties of irreversible protein thermal unfolding measured by DSC. *J. Therm. Anal. Calorim. 80*, 263–270.
(10) Palmieri, M., Malgieri, G., Russo, L., Baglivo, I., Esposito, S., Netti, F., Del Gatto, A., de Paola, I., Zaccaro, L., Pedone, P. V., Isernia, C., Milardi, D., and Fattorusso, R. (2013) Structural Zn(II) Implies a Switch from Fully Cooperative to Partly Downhill Folding in Highly Homologous Proteins. *J. Am. Chem. Soc. 135*, 5220–5228.
(11) Bush, A. I. (2003) The metallobiology of Alzheimer's disease. *Trends Neurosci. 26*, 207–214.
(12) Haass, C., and Selkoe, D. J. (2007) Soluble protein oligomers in neurodegeneration: lessons from the Alzheimer's amyloid beta-peptide. *Nat. Rev. Mol. Cell Biol. 8*, 101–112.
(13) Hawkes, C. A., Ng, V., and McLaurin, J. (2009) Small molecule inhibitors of Aβ-aggregation and neurotoxicity. *Drug Dev. Res. 70*, 111–124.
(14) Wong, H. E., Qi, W., Choi, H.-M., Fernandez, E. J., and Kwon, I. (2011) A safe, blood-brain barrier permeable triphenylmethane dye inhibits amyloid-β neurotoxicity by generating nontoxic aggregates. *ACS Chem. Neurosci. 2*, 645–657.
(15) Soto, P., Griffin, M. A., and Shea, J.-E. (2007) New Insights into the Mechanism of Alzheimer Amyloid-β Fibrillogenesis Inhibition by N-Methylated Peptides. *Biophys. J. 93*, 3015–3025.
(16) Soto, C., Sigurdsson, E. M., Morelli, L., Kumar, R. A., Castaño, E. M., and Frangione, B. (1998) Beta-sheet breaker peptides inhibit fibrillogenesis in a rat brain model of amyloidosis: implications for Alzheimer's therapy. *Nat. Med. 4*, 822–826.
(17) Ghosh, A., Pradhan, N., Bera, S., Datta, A., Krishnamoorthy, J., Jana, N. R., and Bhunia, A. (2017) Inhibition and Degradation of Amyloid Beta (Aβ40) Fibrillation by Designed Small Peptide: A Combined Spectroscopy, Microscopy, and Cell Toxicity Study. *ACS Chem. Neurosci. 8*, 718–722.
(18) B, S. (2007) Antibody-mediated immunotherapy for Alzheimer's disease. *Curr. Opin. Investig. Drugs Lond. Engl. 2000 8*, 519–524.
(19) Frid, P., Anisimov, S. V., and Popovic, N. (2007) Congo red and protein aggregation in neurodegenerative diseases. *Brain Res. Rev. 53*, 135–160.
(20) Yang, D. S., Yip, C. M., Huang, T. H., Chakrabartty, A., and Fraser, P. E. (1999) Manipulating the amyloid-beta aggregation pathway with chemical chaperones. *J. Biol. Chem. 274*, 32970–32974.
(21) Diomede, L., Rigacci, S., Romeo, M., Stefani, M., and Salmona, M. (2013) Oleuropein Aglycone Protects Transgenic C. elegans Strains Expressing Aβ42 by Reducing Plaque Load and Motor Deficit. *PLOS ONE 8*, e58893.
(22) Martorell, M., Forman, K., Castro, N., Capó, X., Tejada, S., and Sureda, A. (2016) Potential Therapeutic Effects of Oleuropein Aglycone in Alzheimer's Disease. *Curr. Pharm. Biotechnol. 17*, 994–1001.

(23) Diomede, L., Cassata, G., Fiordaliso, F., Salio, M., Ami, D., Natalello, A., Doglia, S. M., De Luigi, A., and Salmona, M. (2010) Tetracycline and its analogues protect Caenorhabditis elegans from β amyloid-induced toxicity by targeting oligomers. *Neurobiol. Dis. 40*, 424–431.
(24) Attanasio, F., Convertino, M., Magno, A., Caflisch, A., Corazza, A., Haridas, H., Esposito, G., Cataldo, S., Pignataro, B., Milardi, D., and Rizzarelli, E. (2013) Carnosine Inhibits Aβ42 Aggregation by Perturbing the H-Bond Network in and around the Central Hydrophobic Cluster. *ChemBioChem 14*, 583–592.
(25) Yang, F., Lim, G. P., Begum, A. N., Ubeda, O. J., Simmons, M. R., Ambegaokar, S. S., Chen, P. P., Kayed, R., Glabe, C. G., Frautschy, S. A., and Cole, G. M. (2005) Curcumin inhibits formation of amyloid beta oligomers and fibrils, binds plaques, and reduces amyloid in vivo. *J. Biol. Chem. 280*, 5892–5901.
(26) McLaurin, J., Golomb, R., Jurewicz, A., Antel, J. P., and Fraser, P. E. (2000) Inositol Stereoisomers Stabilize an Oligomeric Aggregate of Alzheimer Amyloid β Peptide and Inhibit Aβ-induced Toxicity. *J. Biol. Chem. 275*, 18495–18502.
(27) McLaurin, J., Kierstead, M. E., Brown, M. E., Hawkes, C. A., Lambermon, M. H. L., Phinney, A. L., Darabie, A. A., Cousins, J. E., French, J. E., Lan, M. F., Chen, F., Wong, S. S. N., Mount, H. T. J., Fraser, P. E., Westaway, D., and St George-Hyslop, P. (2006) Cyclohexanehexol inhibitors of Aβ aggregation prevent and reverse Alzheimer phenotype in a mouse model. *Nat. Med. 12*, 801–808.
(28) Lolicato, F., Raudino, A., Milardi, D., and La Rosa, C. (2015) Resveratrol interferes with the aggregation of membrane-bound human-IAPP: a molecular dynamics study. *Eur. J. Med. Chem. 92*, 876–881.
(29) Hyung, S.-J., DeToma, A. S., Brender, J. R., Lee, S., Vivekanandan, S., Kochi, A., Choi, J.-S., Ramamoorthy, A., Ruotolo, B. T., and Lim, M. H. (2013) Insights into antiamyloidogenic properties of the green tea extract (−)-epigallocatechin-3-gallate toward metal-associated amyloid-β species. *Proc. Natl. Acad. Sci. 110*, 3743–3748.
(30) La Grange, L., Wang, M., Watkins, R., Ortiz, D., Sanchez, M. E., Konst, J., Lee, C., and Reyes, E. (1999) Protective effects of the flavonoid mixture, silymarin, on fetal rat brain and liver. *J. Ethnopharmacol. 65*, 53–61.
(31) Wang, M.-J., Lin, W.-W., Chen, H.-L., Chang, Y.-H., Ou, H.-C., Kuo, J.-S., Hong, J.-S., and Jeng, K.-C. G. (2002) Silymarin protects dopaminergic neurons against lipopolysaccharide-induced neurotoxicity by inhibiting microglia activation. *Eur. J. Neurosci. 16*, 2103–2112.
(32) Cheng, B., Gong, H., Li, X., Sun, Y., Zhang, X., Chen, H., Liu, X., Zheng, L., and Huang, K. (2012) Silibinin inhibits the toxic aggregation of human islet amyloid polypeptide. *Biochem. Biophys. Res. Commun. 419*, 495–499.
(33) Cheng, B., Gong, H., Xiao, H., Petersen, R. B., Zheng, L., and Huang, K. (2013) Inhibiting toxic aggregation of amyloidogenic proteins: a therapeutic strategy for protein misfolding diseases. *Biochim. Biophys. Acta 1830*, 4860–4871.
(34) Gazák, R., Svobodová, A., Psotová, J., Sedmera, P., Prikrylová, V., Walterová, D., and Kren, V. (2004) Oxidised derivatives of silybin and their antiradical and antioxidant activity. *Bioorg. Med. Chem. 12*, 5677–5687.
(35) Lu, P., Mamiya, T., Lu, L., Mouri, A., Zou, L., Nagai, T., Hiramatsu, M., Ikejima, T., and Nabeshima, T. (2009) Silibinin prevents amyloid β peptide-induced memory impairment and oxidative stress in mice. *Br. J. Pharmacol. 157*, 1270–1277.
(36) Yin, F., Liu, J., Ji, X., Wang, Y., Zidichouski, J., and Zhang, J. (2011) Silibinin: A novel inhibitor of Aβ aggregation. *Neurochem. Int. 58*, 399–403.
(37) Di Fabio, G., Romanucci, V., Di Marino, C., De Napoli, L., and Zarrelli, A. (2013) A rapid and simple chromatographic separation of diastereomers of silibinin and their oxidation to produce 2,3-dehydrosilybin enantiomers in an optically pure form. *Planta Med. 79*, 1077–1080.

(38) Di Fabio, G., Romanucci, V., De Nisco, M., Pedatella, S., Di Marino, C., and Zarrelli, A. (2013) Microwave-assisted oxidation of silibinin: a simple and preparative method for the synthesis of improved radical scavengers. *Tetrahedron Lett. 54*, 6279–6282.
(39) Naletova, I., Nicoletti, V. G., Milardi, D., Pietropaolo, A., and Grasso, G. (2016) Copper, differently from zinc, affects the conformation, oligomerization state and activity of bradykinin. *Met. Integr. Biometal Sci. 8*, 750–761.
(40) Grasso, G., Lanza, V., Malgieri, G., Fattorusso, R., Pietropaolo, A., Rizzarelli, E., and Milardi, D. (2015) The insulin degrading enzyme activates ubiquitin and promotes the formation of K48 and K63 diubiquitin. *Chem. Commun. 51*, 15724–15727.
(41) Wu, Y., Cao, Z., Klein, W. L., and Luo, Y. (2010) Heat shock treatment reduces beta amyloid toxicity in vivo by diminishing oligomers. *Neurobiol. Aging 31*, 1055–1058.
(42) Wu, Y., Wu, Z., Butko, P., Christen, Y., Lambert, M. P., Klein, W. L., Link, C. D., and Luo, Y. (2006) Amyloid-beta-induced pathological behaviors are suppressed by Ginkgo biloba extract EGb 761 and ginkgolides in transgenic Caenorhabditis elegans. *J. Neurosci. Off. J. Soc. Neurosci. 26*, 13102–13113.
(43) Beck, M. W., Derrick, J. S., Kerr, R. A., Oh, S. B., Cho, W. J., Lee, S. J. C., Ji, Y., Han, J., Tehrani, Z. A., Suh, N., Kim, S., Larsen, S. D., Kim, K. S., Lee, J.-Y., Ruotolo, B. T., and Lim, M. H. (2016) Structure-mechanism-based engineering of chemical regulators targeting distinct pathological factors in Alzheimer's disease. *Nat. Commun. 7*, 13115.
(44) LeVine, H. (1993) Thioflavine T interaction with synthetic Alzheimer's disease beta-amyloid peptides: detection of amyloid aggregation in solution. *Protein Sci. Publ. Protein Soc. 2*, 404–410.
(45) Goldsbury, C., Baxa, U., Simon, M. N., Steven, A. C., Engel, A., Wall, J. S., Aebi, U., and Müller, S. A. (2011) Amyloid Structure and Assembly: Insights from Scanning Transmission Electron Microscopy. *J. Struct. Biol. 173*, 1–13.
(46) Grasso, G., Mineo, P., Rizzarelli, E., and Spoto, G. (2009) MALDI, AP/MALDI and ESI techniques for the MS detection of amyloid β-peptides. *Int. J. Mass Spectrom. 282*, 50–55.
(47) F, R., J, S., and L, S. (2006) Protein aggregation and amyloidosis: confusion of the kinds? *Curr. Opin. Struct. Biol. 16*, 118–126.
(48) Wang, Q., Yu, X., Patal, K., Hu, R., Chuang, S., Zhang, G., and Zheng, J. (2013) Tanshinones Inhibit Amyloid Aggregation by Amyloid-β Peptide, Disaggregate Amyloid Fibrils, and Protect Cultured Cells. *ACS Chem. Neurosci. 4*, 1004–1015.
(49) Feng, Y., Wang, X., Yang, S., Wang, Y., Zhang, X., Du, X., Sun, X., Zhao, M., Huang, L., and Liu, R. (2009) Resveratrol inhibits beta-amyloid oligomeric cytotoxicity but does not prevent oligomer formation. *Neurotoxicology 30*, 986–995.
(50) Gazit, E. (2002) A possible role for pi-stacking in the self-assembly of amyloid fibrils. *FASEB J. Off. Publ. Fed. Am. Soc. Exp. Biol. 16*, 77–83.
(51) Kai, T., Zhang, L., Wang, X., Jing, A., Zhao, B., Yu, X., Zheng, J., and Zhou, F. (2015) Tabersonine Inhibits Amyloid Fibril Formation and Cytotoxicity of Aβ (1–42). *ACS Chem. Neurosci. 6*, 879–888.
(52) Filippopoulou, K., Papaevgeniou, N., Lefaki, M., Paraskevopoulou, A., Biedermann, D., Křen, V., and Chondrogianni, N. (2017) 2,3-Dehydrosilybin A/B as a pro-longevity and anti-aggregation compound. *Free Radic. Biol. Med. 103*, 256–267.
(53) Kumar, J., Park, K.-C., Awasthi, A., and Prasad, B. (2015) Silymarin extends lifespan and reduces proteotoxicity in C. elegans Alzheimer's model. *CNS Neurol. Disord. Drug Targets 14*, 295–302.
(54) Devi, K. P., Malar, D. S., Braidy, N., Nabavi, S. M., and Nabavi, S. F. (2016) A mini review on the chemistry and neuroprotective effects of silymarin. *Curr. Drug Targets*.
(55) Liu, P., Reed, M. N., Kotilinek, L. A., Grant, M. K. O., Forster, C. L., Qiang, W., Shapiro, S. L., Reichl, J. H., Chiang, A. C. A., Jankowsky, J. L., Wilmot, C. M., Cleary, J. P., Zahs, K. R., and Ashe, K. H. (2015) Quaternary Structure Defines a Large Class of Amyloid-β Oligomers Neutralized by Sequestration. *Cell Rep. 11*, 1760–1771.

(56) Kayed, R., Head, E., Thompson, J. L., McIntire, T. M., Milton, S. C., Cotman, C. W., and Glabe, C. G. (2003) Common structure of soluble amyloid oligomers implies common mechanism of pathogenesis. *Science 300*, 486–489.
(57) Yu, W., He, X., Vanommeslaeghe, K., and MacKerell, A. D. (2012) Extension of the CHARMM general force field to sulfonyl-containing compounds and its utility in biomolecular simulations. *J. Comput. Chem. 33*, 2451–2468.
(58) Vivekanandan, S., Brender, J. R., Lee, S. Y., and Ramamoorthy, A. (2011) A partially folded structure of amyloid-beta(1-40) in an aqueous environment. *Biochem. Biophys. Res. Commun. 411*, 312–316.
(59) Zoete, V., Cuendet, M. A., Grosdidier, A., and Michielin, O. (2011) SwissParam: a fast force field generation tool for small organic molecules. *J. Comput. Chem. 32*, 2359–2368.
(60) Besler, B. H., Merz, K. M., and Kollman, P. A. (1990) Atomic charges derived from semiempirical methods. *J. Comput. Chem. 11*, 431–439.
(61) Singh, U. C., and Kollman, P. A. (1984) An approach to computing electrostatic charges for molecules. *J. Comput. Chem. 5*, 129–145.
(62) Mahoney, M. W., and Jorgensen, W. L. (2000) A five-site model for liquid water and the reproduction of the density anomaly by rigid, nonpolarizable potential functions. *J. Chem. Phys. 112*, 8910–8922.
(63) Nosé, S. (1984) A unified formulation of the constant temperature molecular dynamics methods. *J. Chem. Phys. 81*, 511–519.
(64) Hoover, W. G. (1985) Canonical dynamics: Equilibrium phase-space distributions. *Phys. Rev. A 31*, 1695–1697.
(65) Parrinello, M., and Rahman, A. (1981) Polymorphic transitions in single crystals: A new molecular dynamics method. *J. Appl. Phys. 52*, 7182–7190.
(66) Nosé, S., and Klein, M. L. (1983) Constant pressure molecular dynamics for molecular systems. *Mol. Phys. 50*, 1055–1076.
(67) Darden, T., York, D., and Pedersen, L. (1993) Particle mesh Ewald: An N·log(N) method for Ewald sums in large systems. *J. Chem. Phys. 98*, 10089–10092.
(68) Hess, B., Bekker, H., Berendsen, H. J. C., and Fraaije, J. G. E. M. (1997) LINCS: A linear constraint solver for molecular simulations. *J. Comput. Chem. 18*, 1463–1472.
(69) Abraham, M. J., Murtola, T., Schulz, R., Páll, S., Smith, J. C., Hess, B., and Lindahl, E. (2015) GROMACS: High performance molecular simulations through multi-level parallelism from laptops to supercomputers. *SoftwareX 1*, 19–25.
(70) Humphrey, W., Dalke, A., and Schulten, K. (1996) VMD: visual molecular dynamics. *J. Mol. Graph. 14*, 33–38, 27–28.

Table of content

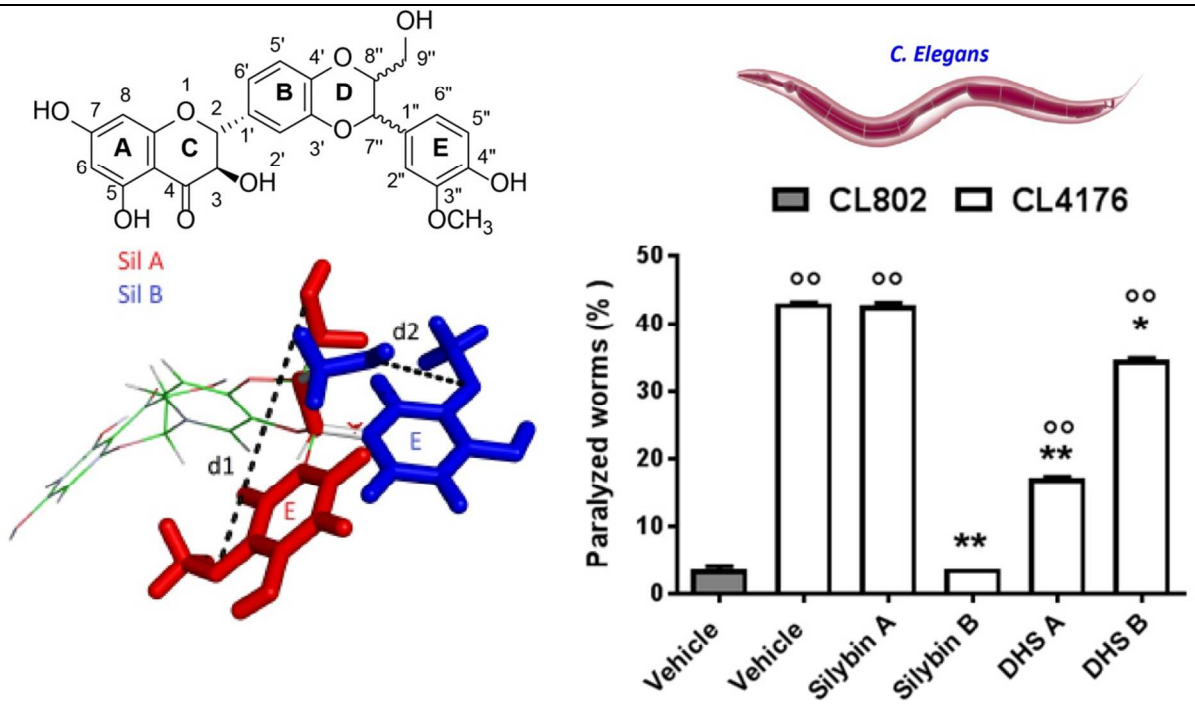

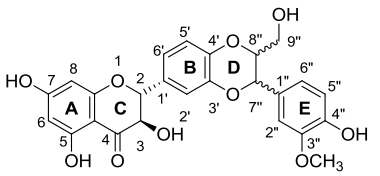

Silibinin

≡

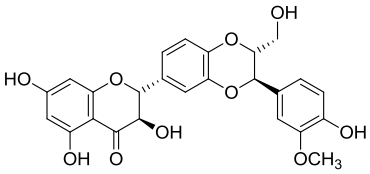

Silybin A (**Sil A**)
(2*R*, 3*R*, 7"*R*, 8"*R*)

+

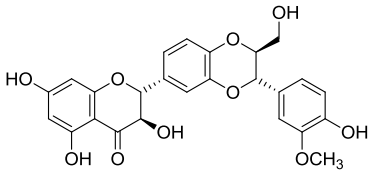

Silybin B (**Sil B**)
(2*R*, 3*R*, 7"*S*, 8"*S*)

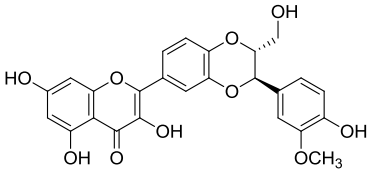

2,3-dehydrosilybin A (**DHS A**)

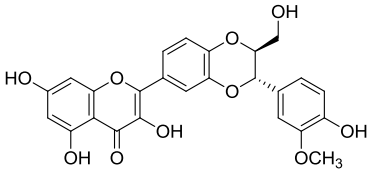

2,3-dehydrosilybin B (**DHS B**)

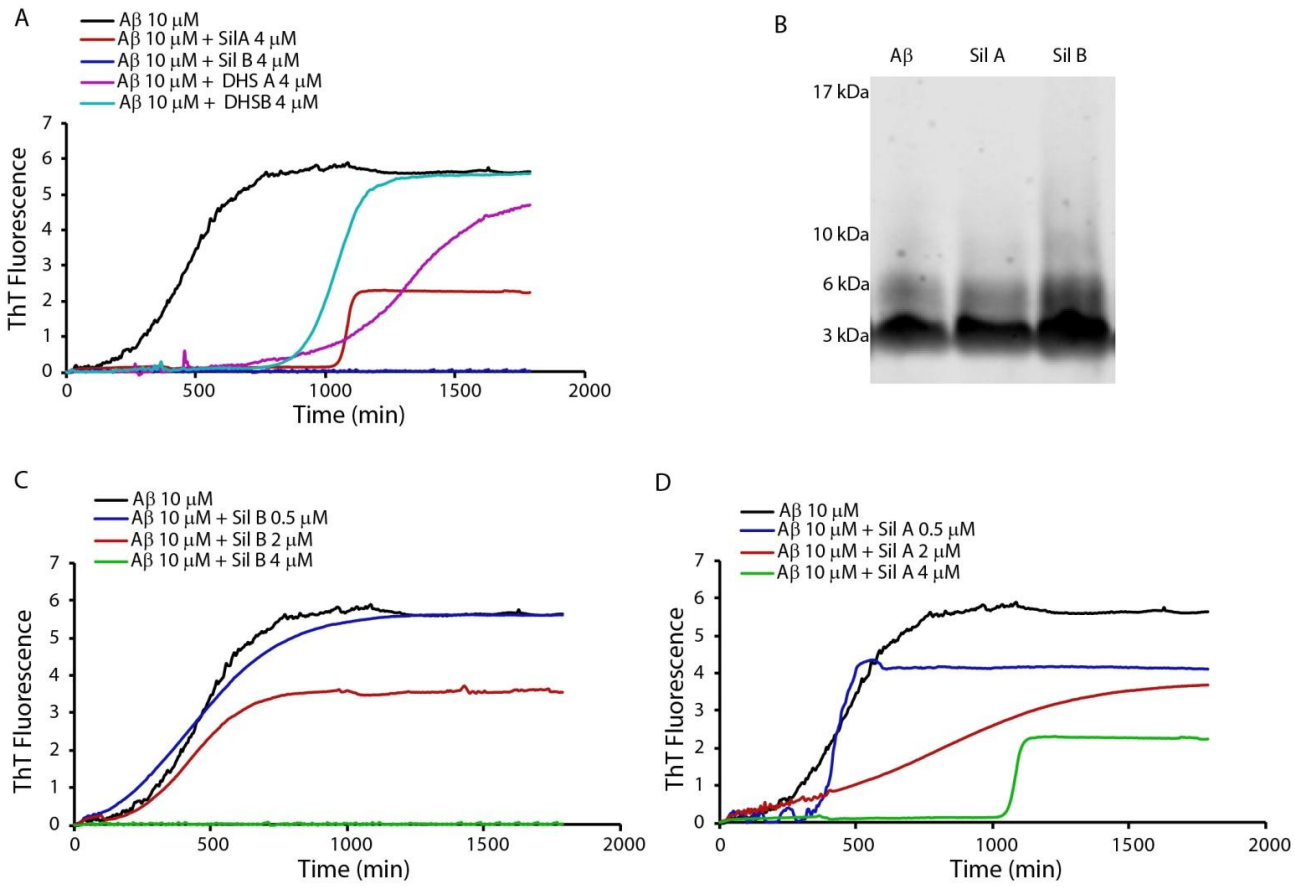
A
Aβ 10 μM
Aβ 10 μM + SilA 4 μM
Aβ 10 μM + Sil B 4 μM
Aβ 10 μM + DHS A 4 μM
Aβ 10 μM + DHSB 4 μM
ThT Fluorescence
Time (min)
B
Aβ
Sil A
Sil B
17 kDa
10 kDa
6 kDa
3 kDa
C
Aβ 10 μM
Aβ 10 μM + Sil B 0.5 μM
Aβ 10 μM + Sil B 2 μM
Aβ 10 μM + Sil B 4 μM
ThT Fluorescence
Time (min)
D
Aβ 10 μM
Aβ 10 μM + Sil A 0.5 μM
Aβ 10 μM + Sil A 2 μM
Aβ 10 μM + Sil A 4 μM
ThT Fluorescence
Time (min)

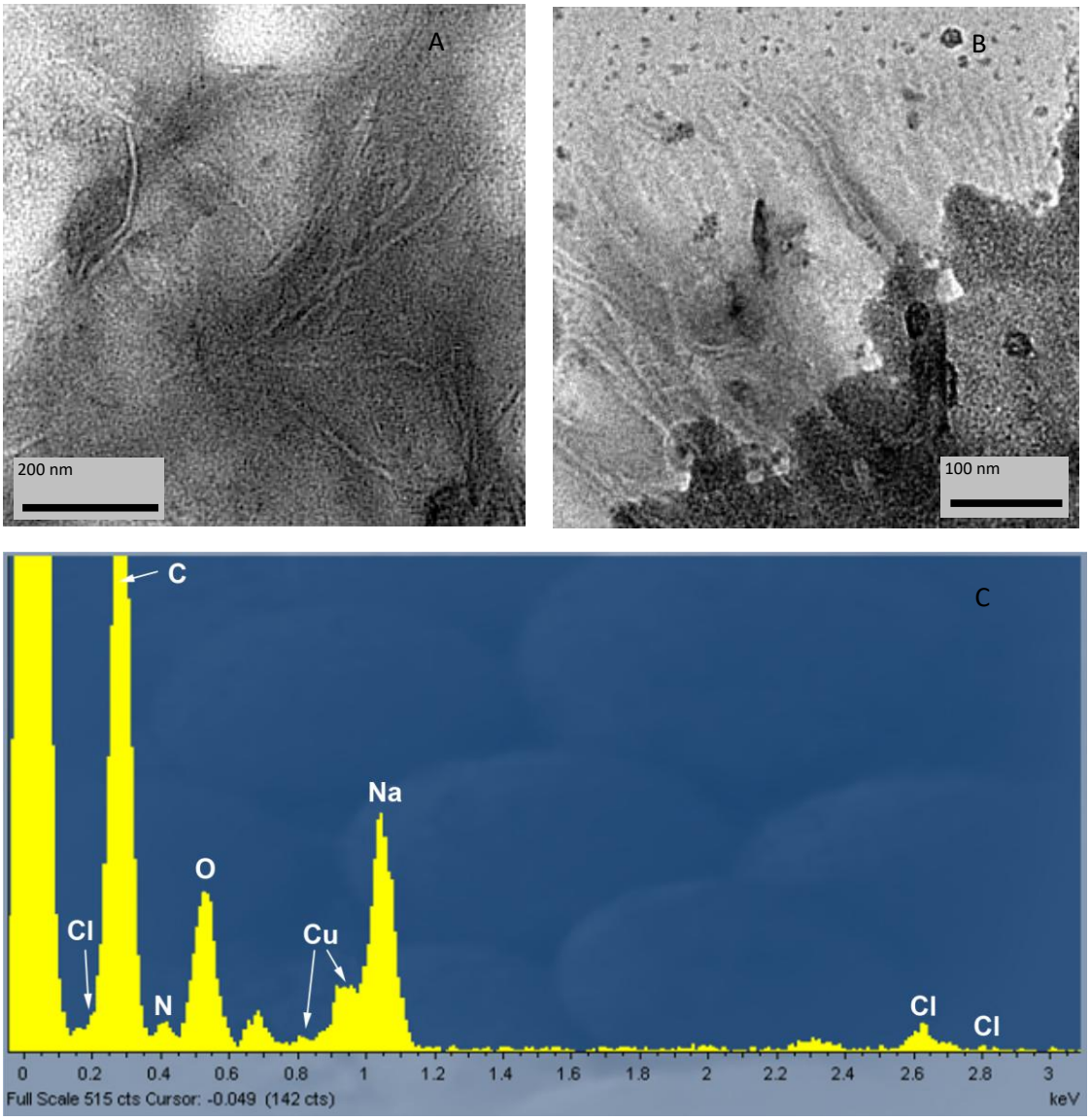
A
200 nm
B
100 nm
C
C
Cl
N
O
Cu
Na
Cl
Cl
0
0.2
0.4
0.6
0.8
1
1.2
1.4
1.6
1.8
2
2.2
2.4
2.6
2.8
3
Full Scale 515 cts Cursor: -0.049 (142 cts)
keV

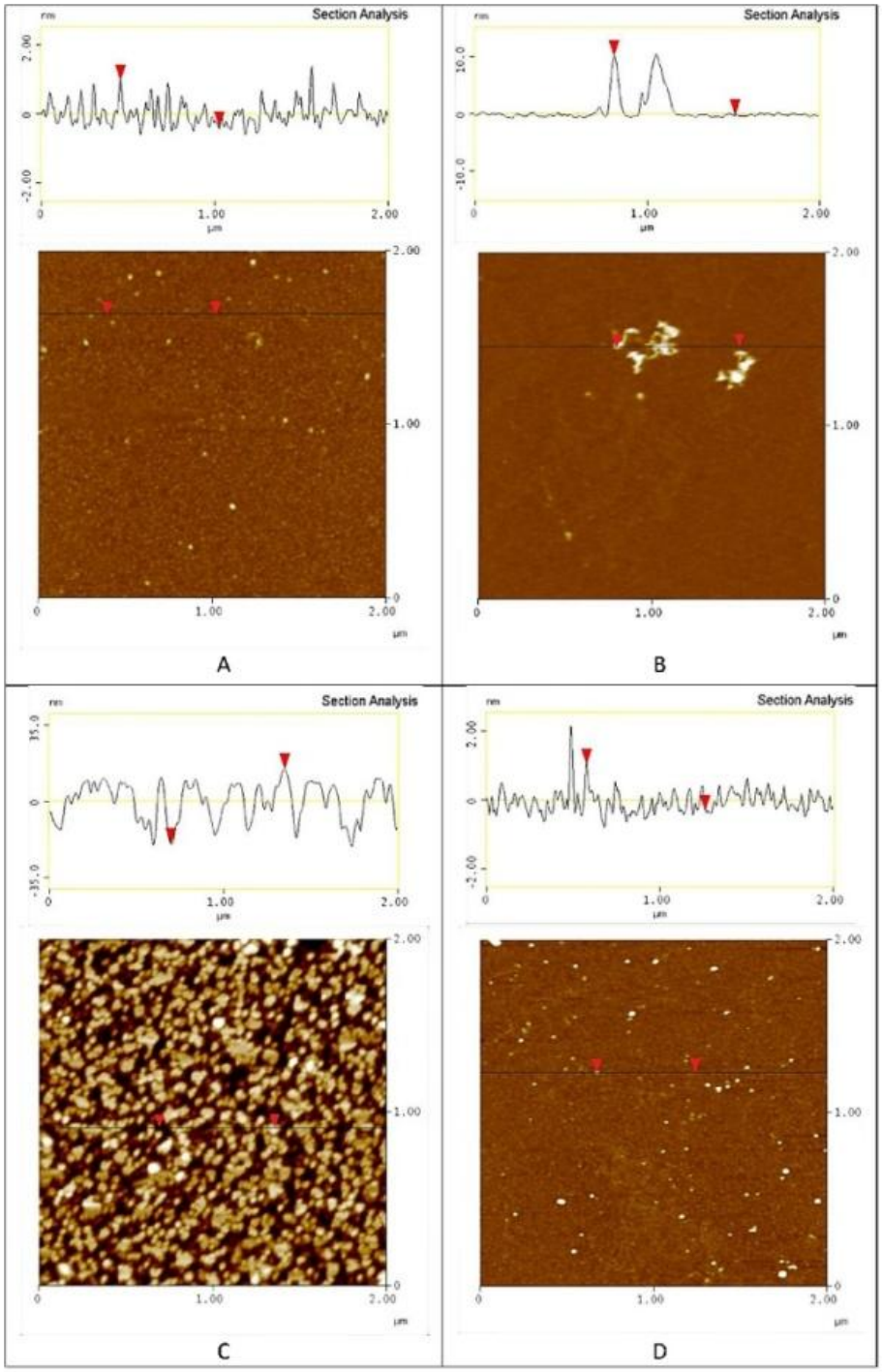
Section Analysis
A
Section Analysis
B
Section Analysis
C
Section Analysis
D

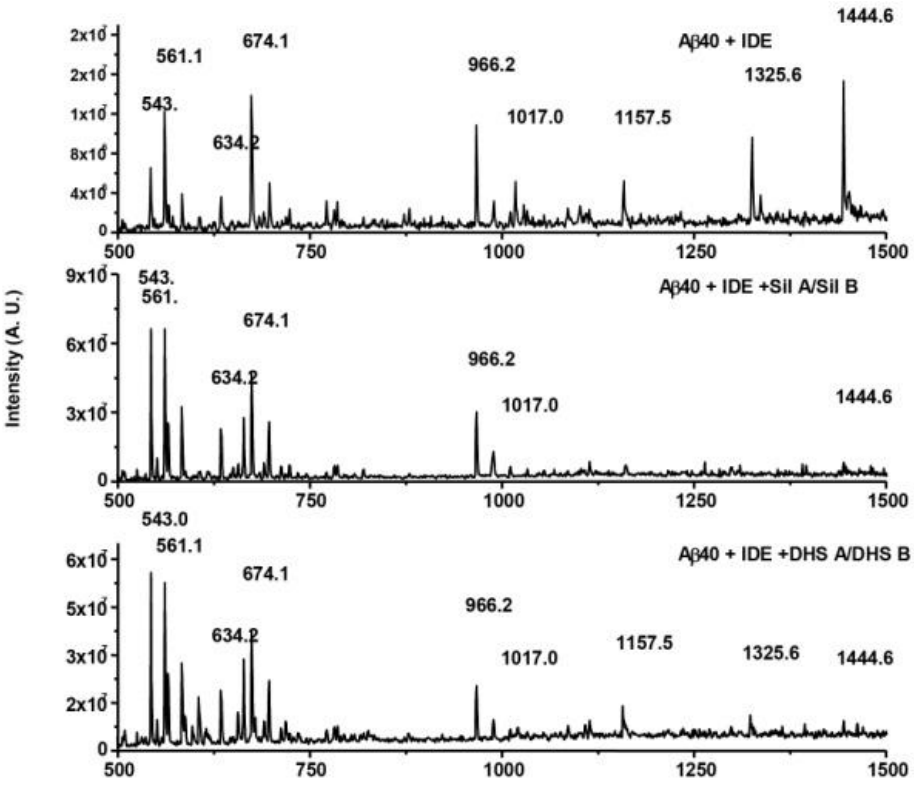
Intensity (A. U.)
Aβ40 + IDE
561.1
674.1
543.
634.2
966.2
1017.0
1157.5
1325.6
1444.6
Aβ40 + IDE +SII A/SII B
543.
561.
674.1
634.2
966.2
1017.0
1444.6
Aβ40 + IDE +DHS A/DHS B
543.0
561.1
674.1
634.2
966.2
1017.0
1157.5
1325.6
1444.6
500
750
1000
1250
1500

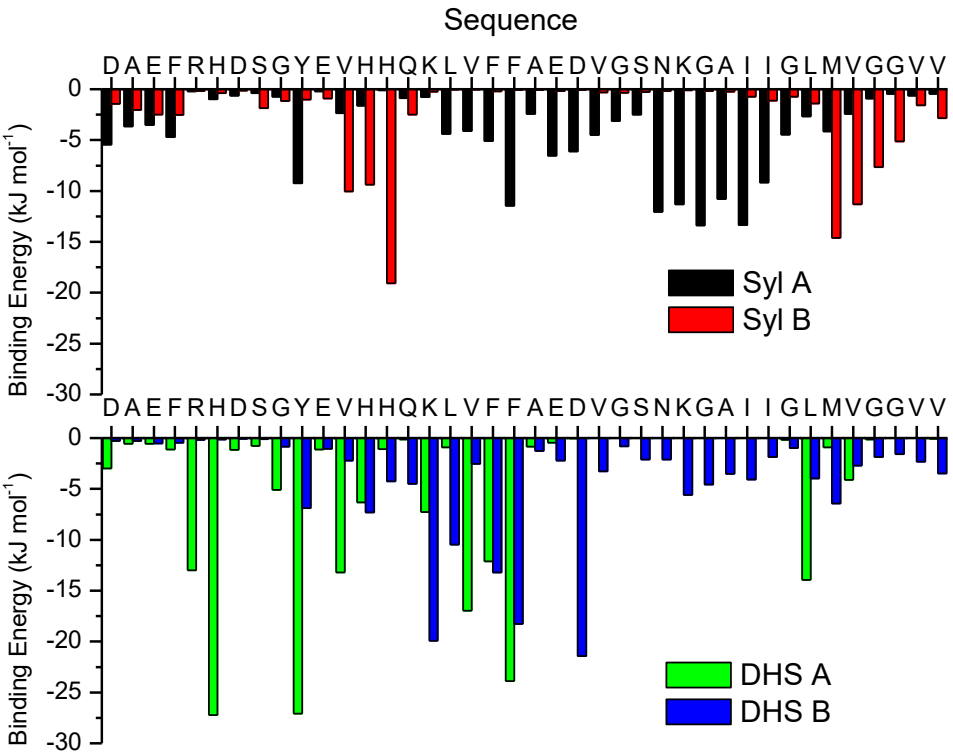
Sequence
D A E F R H D S G Y E V H H Q K L V F F A E D V G S N K G A I I G L M V G G V V
0
-5
-10
-15
-20
-25
-30
Binding Energy (kJ mol-1)
Syl A
Syl B
D A E F R H D S G Y E V H H Q K L V F F A E D V G S N K G A I I G L M V G G V V
0
-5
-10
-15
-20
-25
-30
Binding Energy (kJ mol-1)
DHS A
DHS B

A

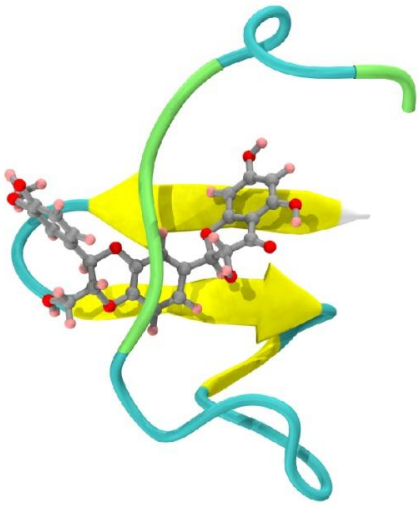

B

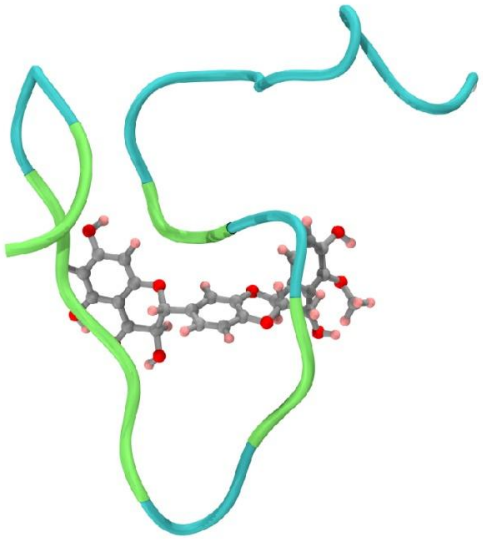

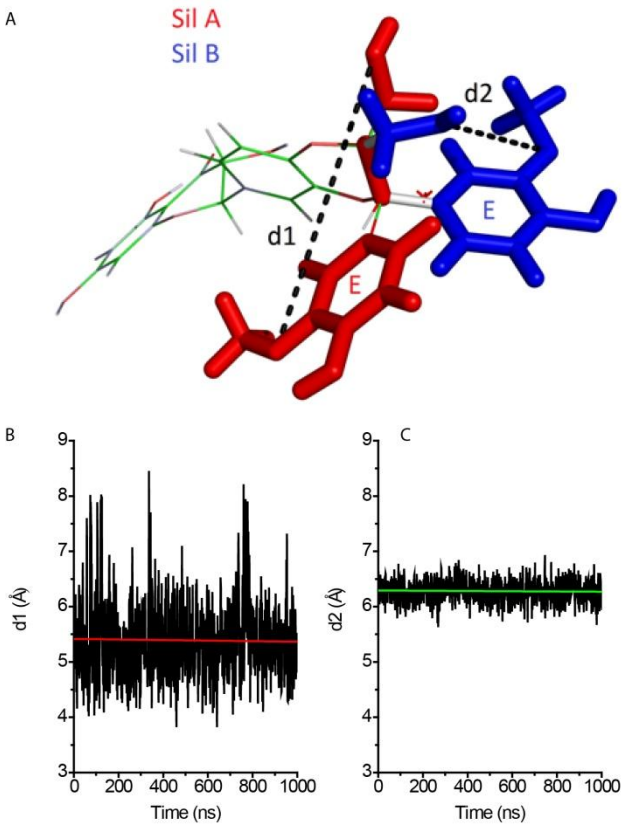
A
Sil A
Sil B
d2
d1
E
E
B
C
d1 (Å)
d2 (Å)
Time (ns)
Time (ns)

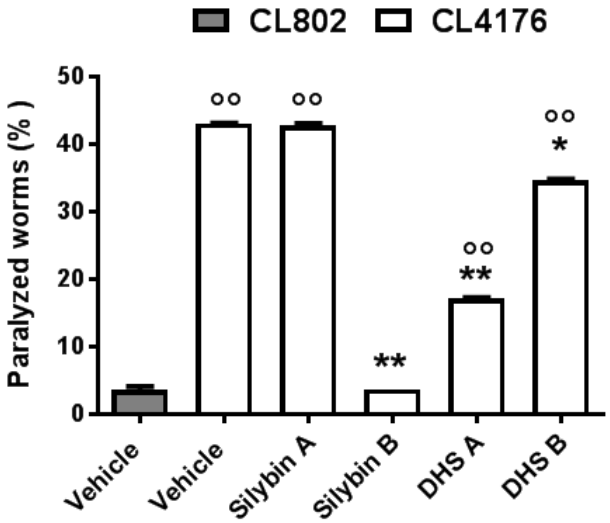
CL802
CL4176
Paralyzed worms (%)
50
40
30
20
10
0
°°
°°
°°
*
°°
**
**
Vehicle
Vehicle
Silybin A
Silybin B
DHS A
DHS B

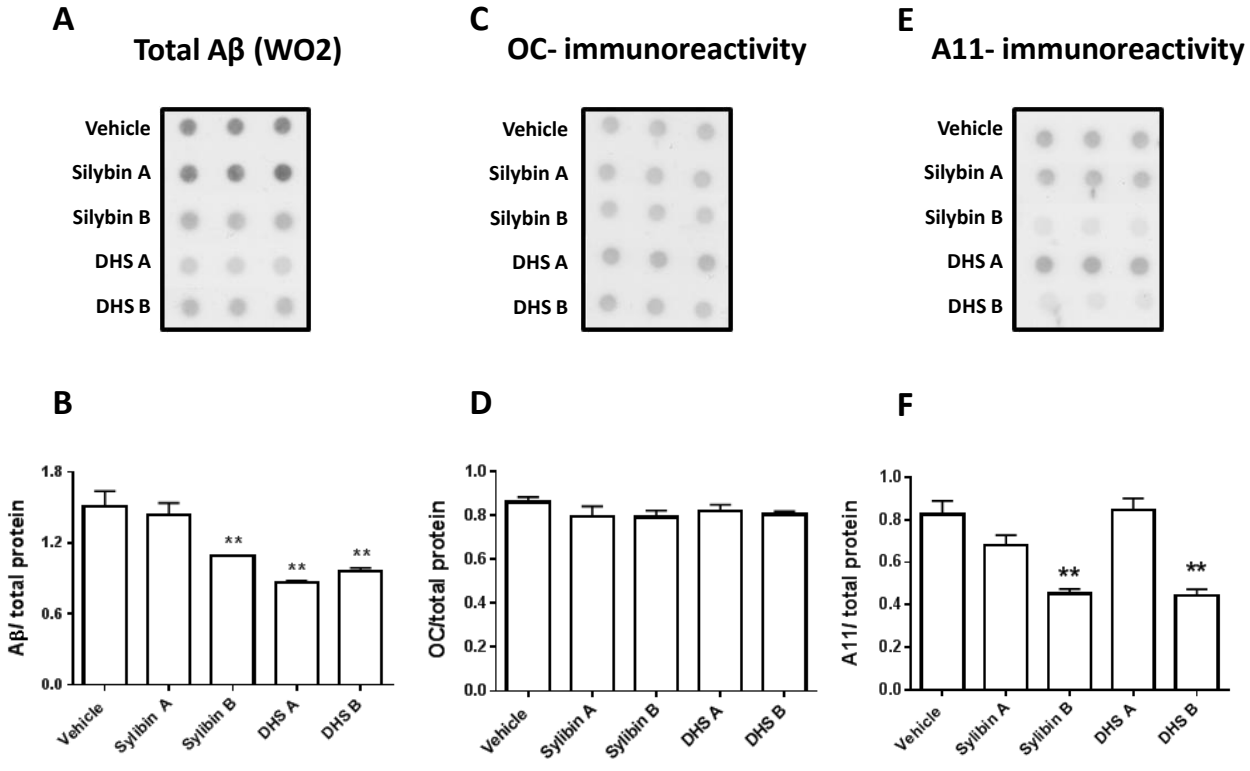
A
Total Aβ (WO2)
Vehicle
Silybin A
Silybin B
DHS A
DHS B
C
OC- immunoreactivity
Vehicle
Silybin A
Silybin B
DHS A
DHS B
E
A11- immunoreactivity
Vehicle
Silybin A
Silybin B
DHS A
DHS B
B
Aβ/ total protein
1.8
1.2
0.6
0.0
**
**
**
Vehicle
Sylibin A
Sylibin B
DHS A
DHS B
D
OC/total protein
1.0
0.8
0.6
0.4
0.2
0.0
Vehicle
Sylibin A
Sylibin B
DHS A
DHS B
F
A11/ total protein
1.0
0.8
0.6
0.4
0.2
0.0
**
**
Vehicle
Sylibin A
Sylibin B
DHS A
DHS B